Control of ATRIAS in Three Dimensions: Walking as a Forced-Oscillation Problem

Siavash Rezazadeh[1] and Jonathan W. Hurst[2]

Abstract

In this paper, we present a new controller for stable and robust walking control of ATRIAS, an underactuated bipedal robot designed based on the Spring-Loaded Inverted Pendulum (SLIP) model. We propose a forced-oscillation scheme for control of vertical motion, which we prove to be stable and contractive. Moreover, we prove that through some mild assumptions, the dynamics of the system can be written in a hierarchical form that decouples the stability analyses of the horizontal and vertical directions. We leverage these properties to find a stabilizing class of functions for foot placement. The torso control is also proved to be decoupled using singular perturbation theory and is stabilized through a feedback linearization controller. We also take advantage of the proposed framework's flexibility and extend it to include a new reflex-based uneven-terrain walking control scheme. We test the controller for various desired walking speeds (0 to 2.5 m/s), for stepping up and down unexpected obstacles (15 cm), and for high-speed walking on a random uneven terrain (up to 10 cm of step-ups and step-downs and up to 1.8 m/s). The results show successful performance of the controller and its stability and robustness against various perturbations.

Keywords

Legged robots, Locomotion, Forced Oscillation, Stability

1 Introduction

Control of a legged robot that is not statically stable is a challenging problem, but it is a crucial step towards understanding the nature of the dynamic phenomena that humans and animals utilize for their stable and efficient locomotion. In this paper, we address this problem through design and test of a walking controller for ATRIAS, a heavily underactuated bipedal robot, whose main features enable it to serve as an embodiment of the Spring-Loaded Inverted Pendulum (SLIP) template (Full and Koditschek (1999)) for the study of dynamic bipedal locomotion.

ATRIAS was designed to realize the essential characteristics of the SLIP model and it was shown that it can closely match those traits in practice (Hubicki et al. (2016)). Based on this, we aim to design a controller for the (actuated) SLIP system with maximum stability and robustness against variations in dynamical parameters, including deviations from the ideal model.

Methods based on the SLIP dynamics are often used for trajectory design for fully-actuated robots, wherein the actuators try to simulate the dynamics of SLIP during stance to accommodate a foot placement scheme based on this template (see Garofalo et al. (2012); Wensing and Orin (2013), for example). This approach, although interesting for fully-actuated humanoids, is problematic for underactuated robots, where an exact replication of the SLIP dynamics is usually not possible due to underactuation. For example, the robot gait obtained in Hereid et al. (2014) was quite different from the base SLIP walking gait (the gait frequency was approximately twice the desired SLIP frequency). In Poulakakis and Grizzle (2009), a more realistic approach was taken for the SLIP-based hopping, which was based on the energy stabilization of the SLIP model using an actuator in leg length direction. In a different but related approach, Schmitt and Clark (2009) extended the stability of SLIP from an energy-conserving space to an energy-varying space by using an open-loop, clock-based trajectories in the leg length direction. Historically, one can even return to the pioneering works of Raibert, in which he utilized pneumatic springs for his hopping robot and achieved spectacular results both in 2D and 3D (Raibert (1986)).

Despite these developments on hopping robots, there have been few works demonstrating stable walking of a robot with point feet in 3D, based on SLIP or otherwise. Hybrid Zero Dynamics (HZD) methods have led to remarkable results in 2D (Westervelt et al. (2007); Sreenath et al. (2011); Park et al. (2013); Post and Schmiedeler (2014)), but their extension to 3D has proven not to be straightforward.

In Rezazadeh et al. (2015), we designed a preliminary version of our controller based on forced oscillations caused by feedforward time-based trajectories. The controller resulted in stable walking with ATRIAS and it was able to maintain stability against perturbation such as pushing. Furthermore, its decoupling and time-based paradigms were successfully used in the HZD framework and implemented on ATRIAS (Griffin and Grizzle (2017); Da and Grizzle (2019)) and Durus (Reher et al. (2016)).

In the present work, we complete and significantly advance the ideas and experiments presented in Rezazadeh

[1]University of Denver, Denver, CO, USA
[2]Oregon State University, Corvallis, OR, USA

Corresponding author:
Siavash Rezazadeh, Department of Mechanical & Materials Engineering, University of Denver, 2155 E. Wesley Ave., Denver, CO 80210, USA.
Email: siavash.rezazadeh@du.edu

et al. (2015). At the theoretical level, we prove that through some mild and practical assumptions, the stability analyses in vertical and horizontal directions can be decoupled. Based on this, we prove the stability of the forced oscillations in vertical direction and use it in designing stable controllers for horizontal-plane motion and torso stabilization. In a way, by using our proposed forced-oscillation paradigm and decoupling assumptions, we provide mathematical proofs for a general control framework for foot placement and torso stabilization, which in their most basic forms simplify to Raibert's controllers (Raibert (1986)). Furthermore, we take advantage of the flexibility of the proposed framework and its strong stability characteristics for appending a reflex-based controller to it, which enables the robot to stably walk over uneven terrains.

The organization of the paper is as follows. First, we briefly introduce ATRIAS and the ideas behind its design. The interested reader may refer to our DARPA Robotics Challenge (DRC) report (Hubicki et al. (2018)) for further details on the hardware and software systems of the robot. In Section 3, we address the control design problem as the main theoretical contribution of this work. Formulation, details, and proofs of the controller are presented in this section. Section 4 presents our experimental results for two main tests: zero to high-speed walking/running and blind-walking on obstacles. Through these experiments and their results we show how the controller features operate to lead to stable walking in extreme conditions. At the end, based on the obtained results, we discuss the advantages and limitation of the controller and we suggest a few future directions.

2 ATRIAS: A Bipedal Robot Designed Based on a Reduced-Order Model

2.1 The Spring-Mass Model

It has been long known that despite the wide diversity of size and morphology of legs in different animals, SLIP model is a useful template for explaining the basic characteristics of running and hopping (Blickhan (1989); Blickhan and Full (1993)). More recently, it was shown that human walking can also be described by the bipedal version of SLIP (Geyer et al. (2006)). Other locomotion modes, such as grounded running, were also observed in the range of behaviors of this template (Martinez and Carbajal (2011)).

SLIP model, as shown in Figure 1(a), consists of a point-mass connected to a spring, through which it dynamically interacts with the ground. Parameters θ and l are called leg angle and leg length, respectively. The bipedal version is similarly defined, with two identical springs instead of one (Figure 1(b)). The springs are massless and thus do not affect the dynamics of the system when they are not in contact with the ground.

SLIP model in its basic form does not have an actuator. Hence, most of the methods addressing the stabilization of SLIP essentially control foot placement, or equivalently, touchdown angle. Nevertheless, in works such as Seyfarth et al. (2002); Geyer et al. (2002); Seyfarth (2003); Altendorfer et al. (2004); Schmitt (2006); Ernst et al. (2009); Vejdani et al. (2015), using this simple control input, interesting stabilizing behaviors against various types of uncertainties and perturbations have been observed and discovered.

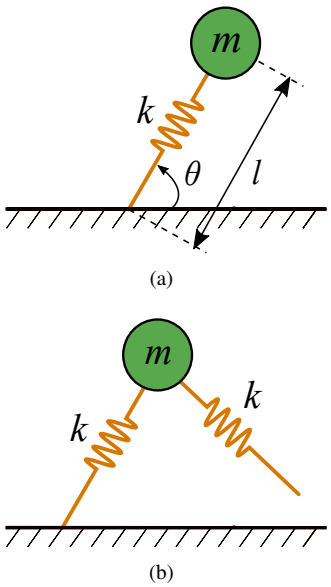

Figure 1. (a) A schematic of SLIP model. (b) The bipedal version of SLIP.

The relation to biological locomotion (as the best examples of legged locomotion) together with such simple stabilizing schemes are not the only factors encouraging the design of legged robots based on the SLIP template. Energy recycling through the spring (rather than through the motor), power amplification for extreme maneuvers, impulse attenuation, and robustness to ground impedance changes are some of other advantageous benefits of a leg design based on the SLIP model (Rezazadeh et al. (2018)). ATRIAS design was founded on such a philosophy.

2.2 ATRIAS

Figure 2 summarizes how the four-bar-linkage mechanism of ATRIAS leg was designed to anchor the SLIP template. The mechanism is an attempt to realize the main features of the SLIP model in a real robot. These features include lumped body mass, spring effectively in leg length direction, point-contact feet, and very light legs (approximately 5% of the mass of the robot). Each spring (Figure 2) is actuated by a brushless DC motor that can swing the leg approximately in the range of $0^\circ < \theta < 180^\circ$, and retract and extend it between $0.32 < l < 0.98$ m. In addition to the two sagittal-plane actuators, each leg is equipped with an abduction-adduction motor, which can move the leg between -20° (adduction) and 30° (abduction).

The sagittal-plane actuators are lumped at the hip, and the frontal-plane motors move them with the leg for adduction and abduction. There are no actuators at the feet and they are completely passive. Each foot consists of a pin joint (which acts as a point contact for the sagittal-plane motion) on top of a two-point-contact, solely to resist against yaw motion, which is an unactuated degree of freedom (DoF). In total, the floating dynamics of the robot has 16 DoF, which is equivalent to 10 degrees of underactuation (DoU). During single-support, these numbers change to 12 DoF and 6 DoU, and during double support to 10 DoF and

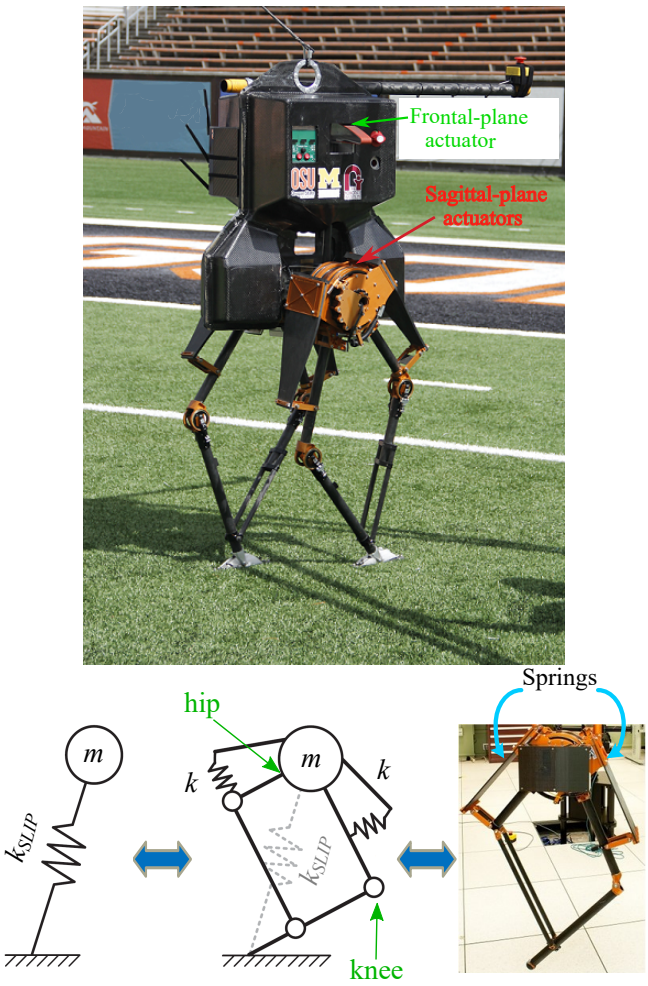

Figure 2. Top: ATRIAS and its actuators. Bottom: From the spring-mass template to ATRIAS's mechanism.

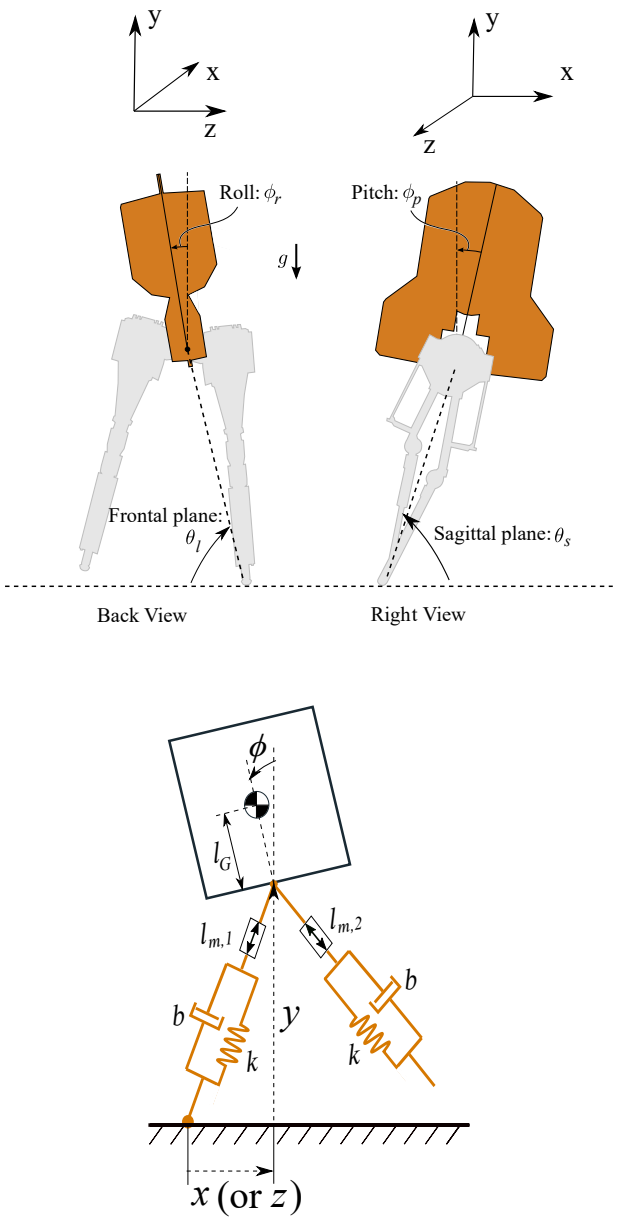

Figure 3. Top: ATRIAS's leg and torso angles in 3D. Note that we drop the subscripts whenever the equations apply to both sagittal and frontal motions or to both roll and pitch rotations. Bottom: View normal to the xy (or yz) plane, and with pitch or roll torso angle ϕ.

4 DoU. The underactuated nature of the mechanism is analogous with the template's energy-conservative essence, which inspires minimal intervention of the actuators. This can lead to designing lighter robots (Rezazadeh et al. (2018)), as well as a better understanding of control paradigms that, despite underactuation, can result in stable locomotion and potentially improve the efficiency of legged systems. See Rezazadeh et al. (2015); Hubicki et al. (2016) for further details on design and specifications of ATRIAS.

3 Control Design

Based on the fact that ATRIAS was designed in a sufficiently faithful way to the defining characteristics of a spring-mass system, we establish our walking control design on this template and use it as a starting point. Analogous with the approach presented in Rezazadeh and Hurst (2015), we start from a reduced-order model and try to synthesize a paradigm that is sufficiently robust to unmodeled dynamics when it is translated to the full-order robot.

3.1 Control Model

Figure 3 depicts the model based on which our walking controller is designed. The model consists of a torso with the center of mass (CoM) above the hip and a diagonal inertia matrix I_t. The torso coordinates are the standard body-fixed yaw-roll-pitch coordinates, with yaw around the y (vertical) axis. The model has two massless compliant legs, each of which with a linear damper as well as an actuator that changes the neutral length of the spring. Hence:

Assumption 1. *The legs are massless and agnostic to the direction of motion in the horizontal plane.*

The invariance of leg kinematics in different directions is in accordance with the standard 3D SLIP (see Wu and Geyer (2013), for example). However, in the case of a robot like ATRIAS in which the hips do not coincide in the frontal plane (each hip is 0.18 m off-center), this assumption is not immediately justified. We will return to this in Remark 9 and show that the approximation is expected to have little effect on the control design.

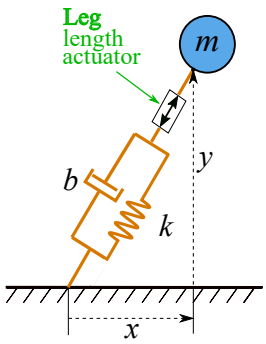

Figure 4. Spring-mass system with damping and a leg-length actuator.

Next, we assume that the feet (two-point-contact feet in the case of ATRIAS) provide sufficient friction forces to prevent the yaw motion. Therefore:

Assumption 2. *The yaw motion is constrained. That is,* $\dot{\phi}_{yaw} \equiv 0$.

Although the problem can be formulated for the general case of Figure 3 directly, let us consider the torso as a point mass for the first stage of the control design. This choice together with the direction invariance from Assumption 1 leads us to consider a model closer to the standard 2D SLIP model (albeit with damping and actuation), as depicted in Figure 4.

It has long been known that the dynamics of SLIP during stance are not integrable (Whittaker (1917); Geyer et al. (2005)). For this reason, several different assumptions in the SLIP hopping studies have been presented in order to resolve this problem. In Schwind and Koditschek (1995), the effect of gravity was neglected and the angular momentum during stance was considered constant. The assumption in De and Koditschek (2015) was even stronger, where in addition to eliminating gravity, the angular velocity during stance was considered constant. Geyer was able to integrate the hopping dynamics by introducing a pair of milder assumptions (Geyer et al. (2005)). Specifically, it was assumed that 1) the deviation from the vertical axis during stance is small, and 2) the spring deflection is small compared to its neutral length.

It is worth noting that because of the double-support phase in walking, the angular momentum around one toe is not only changed by gravity, but also by the force of the other leg. Therefore, Schwind's assumption is likely to lead to greater errors compared to the hopping case. On the other hand, Geyer's assumptions are even more relevant for walking than hopping, because 1) the legs typically sweep smaller angles than forward hopping/running during stance, and 2) spring deflection is smaller due to smaller stance forces (usually about a third of running/hopping forces). Nevertheless, in our control design framework, we only use the first assumption:

Assumption 3. *If* θ *is the leg angle in the frontal or sagittal plane, then* $\cos\theta = \cot\theta = \pi/2 - \theta$.

Although the system will not be integrable with this assumption, as we will show, it is sufficient for our stability analyses.

With Assumption 3, we will have $l = y\sin\theta = y$ and $\dot{l} = \dot{y}$. Then the dynamics of the model of Figure 4 can be written as:

$$\begin{cases} m\ddot{x} = F_l\cos\theta = F_l\frac{x}{y} \\ m\ddot{y} = F_l\sin\theta - mg = F_l - mg \end{cases} \tag{1}$$

Note that,

$$\begin{aligned} F_l &= k(l_m - l) + b(\dot{l}_m - \dot{l}) \\ &= k(l_m - y) + b(\dot{l}_m - \dot{y}), \end{aligned} \tag{2}$$

where l_m is the displacement of the leg length actuator (which changes the neutral length of the spring). Now, if l_m is independent of x and $\dot{x}$, then the second equation (vertical dynamics) in (1) will be independent of the first equation and the dynamics will be in a hierarchical form. In other words, the control of vertical direction can be designed independently from the horizontal-plane control. This is proven in the following proposition.

Proposition 1. *The stability analyses of any periodic orbit pertaining to a system described by* (1) *and* (2) *with* $\frac{\partial l_m}{\partial x} = \frac{\partial l_m}{\partial \dot{x}} \equiv 0$ *are independent of each other in horizontal and vertical directions.*

Proof. Based on (1), (2), and the assumption imposed on l_m, y evolves independently from x and $\dot{x}$. Therefore, for an arbitrary Poincaré section, we will have: $Y_{i+1} = P_y(Y_i)$, where P_y is the Poincaré map corresponding to y-direction, and Y_i represents the y-direction states in the ith step. Then, by including the x-direction Poincaré map, we can write:

$$\begin{cases} Y_{i+1} = P_y(Y_i) \\ X_{i+1} = P_x(X_i, Y_i) \end{cases} \tag{3}$$

where, similarly, P_x and X_i represent the Poincaré map and the ith-step states in the x direction. The Jacobian can then be obtained as:

$$J_P = \begin{bmatrix} \frac{\partial P_x}{\partial X_i} & \frac{\partial P_x}{\partial Y_i} \\ 0 & \frac{\partial P_y}{\partial Y_i} \end{bmatrix} \tag{4}$$

Since J_p is block-triangular, its eigenvalues are the eigenvalues of the diagonal terms. i.e., $\frac{\partial P_x}{\partial X_i}$ and $\frac{\partial P_y}{\partial Y_i}$. That is, the eigenvalues of the whole dynamics (λ_p) can be decoupled into eigenvalues corresponding to each of x and y directions. This, in turn, means that the stability properties of the two directions are decoupled.

Proposition 1 can greatly simplify the design of a walking controller, which, in turn, facilitates the finding of stronger stabilization schemes. Based on this, in what follows, we design a controller with maximum stability and robustness for vertical motion, considering that it will not affect the horizontal-direction stability.

3.2 Control of Vertical Motion

3.2.1 Feedforward Time-Based Trajectories Control of a 1D system in the vertical direction has a long history in hopping robots. Raibert (1986) used impulsive thrusts provided by pneumatic actuators to achieve stable hopping heights. Koditschek and Buehler (1991) theoretically proved

that this impulsive energy injection scheme indeed leads to stabilization. Since the impulsive thrusts cannot be achieved in electrical actuators and inspired by biological observations, Komsuoglu and Koditschek (2000) proposed the use of a feedforward clock-driven scheme for stable hopping. Similar feedforward schemes were used in hopping robots such as Dashpod (Cham and Cutkosky (2007)) and Salto (Haldane et al. (2016)). This stabilizing behavior of feedforward clock-driven inputs were also observed in other applications, such as juggling (Schaal and Atkeson (1993)) and sliding manipulation (Vose et al. (2012)).

These clock-driven schemes for electrically actuated systems have been attractive and elegant paradigms that can provide stable hopping with minimal sensory feedback. Inspired by this, we found it reasonable to extend these schemes and design a version for the bipedal walking systems. As we will show, it has also other benefits within our framework.

Vertical dynamics in legged locomotion are especially important because state changes (swing to stance and vice versa) depend solely on the attributes of this direction. Touchdown happens when the toe's vertical height becomes zero, and takeoff takes place when the vertical ground reaction force vanishes. Furthermore, unlike hopping where the neutral leg length is usually not changed (unless minimally for energy control), in the case of walking, the foot height has to be controlled through retraction of the leg in order to avoid toe-stubbing. Therefore, unlike the clock-driven schemes cited above, the feedforward trajectory cannot be a simple force input. Rather, it has to be a controlled position trajectory, as l_m in (2) represents. Note that since the legs are massless, during swing phase $l = l_m$ and $\dot{l} = \dot{l}_m$, and thus designing an appropriate l_m trajectory will lead to proper control of the toe height during swing.

Based on the above discussion, we propose a simple sinusoidal scheme for l_m with a phase difference of π:

$$l_{m,1}(t) = \begin{cases} l_0 & \sin\omega t > 0 \\ l_0 + a\sin\omega t & \sin\omega t \leq 0 \end{cases} \tag{5}$$

$$l_{m,2}(t) = \begin{cases} l_0 & \sin\omega t \leq 0 \\ l_0 - a\sin\omega t & \sin\omega t > 0 \end{cases} \tag{6}$$

where subscripts 1 and 2 refer to the leg index, and ω and a are frequency and maximum leg retraction, respectively. Using (5) and (6), the neutral length of the spring is held constant in half of the period (*roughly* the stance phase) and thus the leg acts as a passive system. In the other half of the period, the leg retracts to the maximum retraction a and then extends back to the neutral length. Figure 5 depicts an example of such a set of trajectories.

3.2.2 Analysis of Vertical Oscillations with the Proposed Feedforward Trajectories Neglecting the flight phase for now, substituting F_l from (2) in the second equation of (1) for $l_{m,1} < l < l_{m,2}$ or $l_{m,2} < l < l_{m,1}$ (single support), and rearranging terms results in:

$$m\ddot{y} + b\dot{y} + ky = kl_0 - mg \tag{7}$$

which is essentially the dynamics of a free-oscillation system. Similarly, for double support ($l < \min\{l_{m,1}, l_{m,2}\}$):

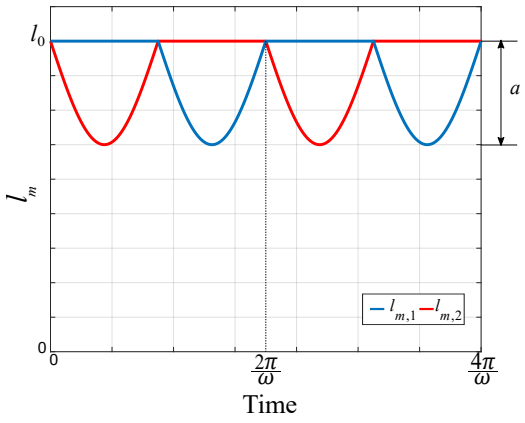

Figure 5. An example of feedforward trajectories of (5) and (6) for two cycles (strides).

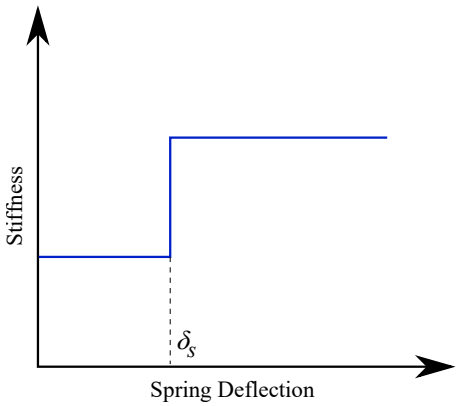

Figure 6. An example of a bilinear stiffness. The stiffness changes when a specific deflection δ_s is reached. Note that although the stiffness is discontinuous, the spring force is still continuous.

$$m\ddot{y} + 2b\dot{y} + 2ky = kl_m + b\dot{l}_m + kl_0 - mg \tag{8}$$

where l_m represents $l_{m,i}$ for the leg that is oscillating at the given instant, i.e. $l_m < l_0$. Equation (8), given that $kl_m + b\dot{l}_m$ is a sinusoidal function (see (6)), is a standard forced oscillation problem. From (7) and (8) one can conclude that the system consists of a sequence of free- and forced-oscillation linear sets of dynamics. Due to different sets of parameters (stiffness and damping) in the two systems, such a system is called a *piecewise linear system* in the literature. The analysis of piecewise linear systems dates back to 1930s in vibration isolation applications (Pogorilyi et al. (2015)). The systems studied in these works usually consisted of a mass-spring-damper with an additional spring that could be engaged when a preset position is reached (Figure 6). The engagement of the additional spring changes the total stiffness, and as a result, the dynamics of the linear system (Fleishman (1965)).

One of the reasons for interesting behaviors of piecewise linear systems is that, although they use two linear springs, they can exhibit the characteristics of nonlinear systems, including chaos (Schulman (1983)). Analogous with this and due to the instantaneous switching between two different sets of dynamics. the analysis of these systems is highly challenging. Despite the simplicity of the equations, solving them typically results in a set of transcendental equations that

cannot be solved analytically. Natsiavas (1989) showed that the forced oscillations of a system such as the one depicted in Figure 6 (with constant damping) leads to a set of six transcendental equations that can further be simplified to a single transcendental equation. The remaining equation then was used for stability analysis. In what follows, we investigate the solution for the forced oscillations of (7) and (8).

Figure 7 displays the steady-state response of the system of equations (7) and (8) for two different values of a, $\omega = 2\pi/0.7$ rad/s, and $l_0 = 0.9$ m. Other parameters are: $m = 62$ kg, $b = 1.5$ N.s/m, and $k = 25000$ N/m, which are chosen based on the parameters of ATRIAS (Rezazadeh et al. (2015)). When a is close to zero (Figure 7(b)), the oscillations are not large enough for the leg retraction to lift the foot off the ground. As a result, the system always remains in the double support phase and oscillates around its static equilibrium $y_{\text{static}} = l_0 - mg/2k$.

When a is sufficiently large (Figure 7(a)), three separate phases can be distinguished in the periodic response: double support for $0 \leq t < t_1$, single support for $t_1 \leq t < t_2$, and again double-support for $t_2 \leq t < \pi/\omega$, where $t_1 \approx 0.008$ s and $t_2 \approx 0.342$ s. Let us name the trajectories corresponding to these segments as y_1, y_2, and y_3, respectively. Before investigating the solutions, we present another assumption:

Assumption 4. *The system, both in single-support and double-support, is underdamped.*

Assumption 4, although not necessary for our analysis and proof, is justified by the design philosophy of the leg based on a spring-mass system (Rezazadeh et al. (2018)), for which one of the prime motivations is efficiency. Hence using a spring with low damping is preferred. The underdamped nature of ATRIAS legs was also shown in Hubicki et al. (2016), where the locked oscillations of the robot on its legs took several steps to damp. Nevertheless, the extension of the analyses and proofs of this section to the overdamped case is straightforward.

Let us define:

$$\begin{cases} \zeta_{ss} = b/2\sqrt{km} & \zeta_{ds} = b/\sqrt{2km} \\ \omega_{n,ss} = \sqrt{k/m} & \omega_{n,ds} = \sqrt{2k/m} \\ \omega_{d,ss} = \omega_{n,ss}\sqrt{1-\zeta_{ss}^2} & \omega_{d,ds} = \omega_{n,ds}\sqrt{1-\zeta_{ds}^2} \end{cases} \tag{9}$$

Following the methodology of Natsiavas (1989), we can write:

$$\begin{aligned} y_1(t) =& e^{-\zeta_{ds}\omega_{n,ds}t}(A_1 \sin\omega_{d,ds}t + B_1 \cos\omega_{d,ds}t) \\ &+ F_1 \sin\omega t + F_2 \cos\omega t + l_0 - \frac{mg}{2k} \end{aligned} \tag{10}$$

$$\begin{aligned} y_2(t) = e^{-\zeta_{ss}\omega_{n,ss}(t-t_1)}&[A_2 \sin\omega_{d,ss}(t-t_1) \\ &+ B_2 \cos\omega_{d,ss}(t-t_1)] \\ &+ l_0 - \frac{mg}{k} \end{aligned} \tag{11}$$

$$\begin{aligned} y_3(t) = e^{-\zeta_{ds}\omega_{n,ds}(t-t_2)}&[A_3 \sin\omega_{d,ds}(t-t_2) \\ &+ B_3 \cos\omega_{d,ds}(t-t_2)] \\ &+ F_1 \sin\omega t + F_2 \cos\omega t + l_0 - \frac{mg}{2k} \end{aligned} \tag{12}$$

where the forced-oscillation coefficients can be computed as:

$$F_1 = -\frac{a(2b^2\omega^2 + 2k^2 - mk\omega^2)}{(2k - m\omega^2)^2 + 4b^2\omega^2} \tag{13}$$

$$F_2 = \frac{amb\omega^3}{(2k - m\omega^2)^2 + 4b^2\omega^2} \tag{14}$$

As such, similar to Pogorilyi et al. (2015), there are eight unknowns that need to be computed from the initial and boundary conditions: $A_1, B_1, A_2, B_2, A_3, B_3, t_1$ and t_2. Two of these eight equations can be obtained from the periodicity of the solution:

$$\begin{cases} y_1(0) = y_3(\pi/\omega) \\ \dot{y}_1(0) = \dot{y}_3(\pi/\omega) \end{cases} \tag{15}$$

Continuity conditions at t_1 and t_2 (corresponding to a C^2 period-1 orbit) leads to four more equations:

$$\begin{cases} y_1(t_1) = y_2(t_1) \\ \dot{y}_1(t_1) = \dot{y}_2(t_1) \\ y_2(t_2) = y_3(t_2) \\ \dot{y}_2(t_2) = \dot{y}_3(t_2) \end{cases} \tag{16}$$

The last two equations are obtained from the time-based input (l_m), which causes phase switching from double-support to single-support and vice versa:

$$\begin{cases} y_1(t_1) = l_0 - a\sin\omega t_1 \\ y_2(t_2) = l_0 - a\sin\omega t_2 \end{cases} \tag{17}$$

In the previous cases of the piecewise linear systems presented in the literature (Natsiavas (1989) and Pogorilyi et al. (2015)), switchings would occur at a fixed position. That is, in these works, the switching condition had the form of $h(y) = 0$. The independence of h from time can be leveraged to reduce the number of equations to one (Natsiavas (1989)) or two (Pogorilyi et al. (2015)). In contrast, (17) presents a set of time-variant switchings in the form of $h(t, y) = 0$, which leads to a much more complicated case with irreducible number of equations. Nevertheless, as we will show in what follows, we can still utilize the special structure of the response to study the stability properties of the system.

3.2.3 Stability of Vertical Oscillations Consider a linear second-order system with an external input $u_i(t)$,

$$\begin{cases} \ddot{y}_i + 2\zeta_i\omega_{n,i}\dot{y}_i + \omega_{n,i}^2 y_i = u_i(t) & t_{i-1} \leq t \leq t_i \\ h_i(t_i, y_i, \dot{y}_i) = 0, \end{cases} \tag{18}$$

which can describe the forms of both single-support and double-support dynamics as in (7) and (8), respectively. The input u_i represents a periodic, bounded, and continuous

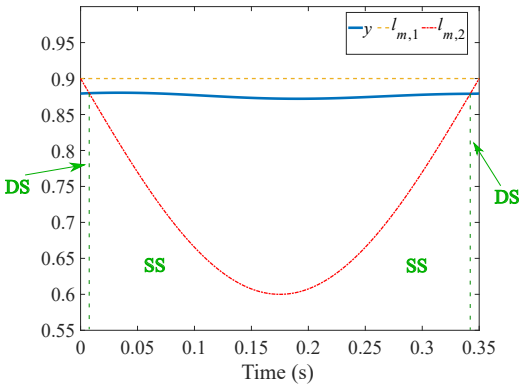

(a)

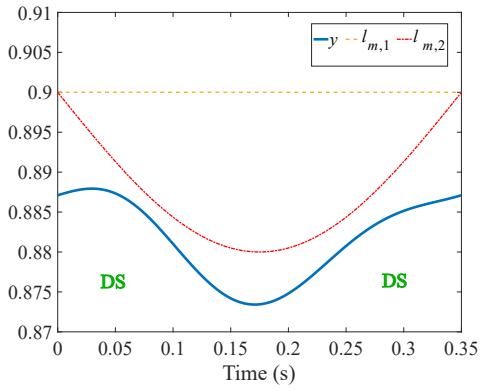

(b)

Figure 7. The period-1 response of the 1D vertical oscillator with two different oscillation amplitudes: (a) $a = 0.3$ m. (b) $a = 0.02$ m. "DS" and "SS" refer to the double support and single support regions of the cycle, respectively.

function defined, for example, by the right hand side of (7) or (8), and $h_i(t_i, y_i, \dot{y}_i) = 0$ is the switching condition (as in (17)) from y_i to y_{i+1}.

Theorem 1. *Consider a hybrid system consisting of a sequence of SS and DS phases, represented by underdamped linear second-order systems $\mathcal{S}_i$, $i = 1, ..., n$. The system is subject to a set of C^0 time-based periodic inputs $u_i(t) : \mathbb{R} \to \mathbb{R}$ and its states are continuous, including at the switching points. Any periodic orbit of this system preserving the sequence of SS and DS phases is stable.*

Proof. Based on Assumption 4, similar to (10)-(12), the solutions for each phase of (18) ($t_{i-1} \leq t \leq t_i$) can be written in the following form:

$$y_i(t) = e^{-\zeta_i \omega_{n,i}(t-t_{i-1})}[A_i \sin \omega_{d,i}(t - t_{i-1}) + B_i \cos \omega_{d,i}(t - t_{i-1})] + w_i(t) \tag{19}$$

where w_i is the particular solution of the differential equation for $u_i(t)$ and is C^2 due to the fact that the system is of relative-degree two. Taking the time derivative from $y_i(t)$ and using the initial conditions at t_{i-1} the constant parameters A_i and B_i can be written as:

$$A_i = \frac{\dot{y}_i(t_{i-1}) + \zeta_i \omega_{n,i}\,(y_i(t_{i-1}) - w_i(t_{i-1})) - \dot{w}_i(t_{i-1})}{\omega_{d,i}} \tag{20}$$

$$B_i = y_i(t_{i-1}) - w_i(t_{i-1}) \tag{21}$$

Now, by defining the state vector for $t_{i-1} \leq t \leq t_i$ as $Y(t) = [y_i(t) \quad \dot{y}_i(t)]^T$, and differentiating it with respect to the initial condition state $Y(t_{i-1}) = [y_i(t_{i-1}) \quad \dot{y}_i(t_{i-1})]^T$, the state transition matrix can be computed:

$$\Phi_i(t, t_{i-1}) = e^{-\zeta_i \omega_{n,i}(t-t_{i-1})} J_i \tag{22}$$

where J_i is a 2×2 matrix independent of the initial conditions and contains combinations of $\sin \omega_{d,i}(t - t_{i-1})$ and $\cos \omega_{d,i}(t - t_{i-1})$. The expression for J_i is omitted for the sake of brevity. The eigenvalues of Φ_i are given by:

$$\lambda_{\Phi,i}(t, t_{i-1}) = e^{-\zeta_i \omega_{n,i}(t-t_{i-1})}[\cos \omega_{d,i}(t - t_{i-1}) \pm j \sin \omega_{d,i}(t - t_{i-1})], \tag{23}$$

which means:

$$|\lambda_1(J_i)| = |\lambda_2(J_i)| = |J_i| = 1 \tag{24}$$

Now, by taking $W_i(t) := [w_i(t) \quad \dot{w}_i(t)]^T$, we will have:

$$Y(t) = \Phi_i(t, t_{i-1})[Y(t_{i-1}) - W_i(t_{i-1})] + W_i(t) \tag{25}$$

and:

$$\dot{Y}(t) = \dot{\Phi}_i(t, t_{i-1})[Y(t_{i-1}) - W_i(t_{i-1})] + \dot{W}_i(t) \tag{26}$$

which, by properties of state transition matrices (see Bernstein (2009), for example) can also be written as:

$$\dot{Y}(t) = \Phi_i(t, t_{i-1})[\dot{Y}(t_{i-1}) - \dot{W}_i(t_{i-1})] + \dot{W}_i(t) \tag{27}$$

Taking variation from (25) at $t = t_i$ with $Y_i := Y(t_i)$ results in:

$$\begin{aligned}\delta Y_i =& \Phi_i(t_i, t_{i-1})[\delta Y_{i-1} - \delta W_i(t_{i-1})] \\ &+ \delta\Phi_i(t_i, t_{i-1})[Y_{i-1} - W_i(t_{i-1})] + \delta W_i(t_i)\end{aligned} \tag{28}$$

Noting that time in Φ_i appears in the form $t - t_{i-1}$, we have:

$$\delta\Phi_i(t, t_{i-1}) = \dot{\Phi}_i(t, t_{i-1})(\delta t - \delta t_{i-1}) \tag{29}$$

Similarly:

$$\delta W_i(t) = \dot{W}_i(t)\delta t \tag{30}$$

Substituting (26), (27), (29), and (30) in (28), we obtain:

$$\delta Y_i = \Phi_i(t_i, t_{i-1})\delta Y_{i-1} + \dot{Y}_i \delta t_i - \Phi_i(t_i, t_{i-1})\dot{Y}_{i-1}\delta t_{i-1} \tag{31}$$

Noting that at the ith transition point we have $h_i(t_i, Y_i) \equiv 0$, we can write:

$$\frac{\partial h_i}{\partial Y_i}\delta Y_i + \frac{\partial h_i}{\partial t_i}\delta t_i = 0 \tag{32}$$

Thereby, δt_i can be obtained in the following form:

$$\delta t_i = H_i \delta Y_i, \tag{33}$$

where $H_i := -\frac{\partial h_i/\partial Y_i}{\partial h_i/\partial t_i}$. Substituting δt_i and $\delta t_{i-1} = H_{i-1}\delta Y_{i-1}$ in (31) and solving for δY_i results in:

$$\delta Y_i = (I - \dot{Y}_i H_i)^{-1} \Phi_i(t_i, t_{i-1})(I - \dot{Y}_{i-1} H_{i-1})\delta Y_{i-1}, \tag{34}$$

where I is the identity matrix. Using (34) recursively leads to:

$$\delta Y_n = (I - \dot{Y}_n H_n)^{-1} \left(\prod_{i=1}^{n} \Phi_i(t_i, t_{i-1}) \right) (I - \dot{Y}_0 H_0)\delta Y_0 \tag{35}$$

Note that the analysis is being performed between $t = 0$ and $t = \frac{\pi}{\omega}$ and the initial and final t's are not changing with variations of the initial conditions. This is often called a stroboscopic Poincaré section, which is an extension of the Poincaré map for the time-varying systems. Hence, $\delta t_0 = \delta t_n = 0$, which is equivalent to $H_0 = H_n = 0$. Using this, we have:

$$\delta Y_n = \left(\prod_{i=1}^{n} \Phi_i(t_i, t_{i-1}) \right) \delta Y_0 \tag{36}$$

This means that the stroboscopic Poincaré map between δY_0 and δY_n corresponds to that of the same sequence of second-order systems with the same switching times (t_is) as the nominal (unperturbed) periodic orbit. The difference is that here the external input (u_i) is absent. For nonzero damping values (i.e., $\zeta_i > 0$), each Φ_i represents a dissipative system that contracts the norm of the initial condition. That is, $\forall \xi \in \mathbb{R}^2, i \in \{1, ..., n\}, \quad ||\Phi_i(t_i, t_{i-1})\xi|| < ||\xi||$. Since there is no external input action in (36), it is immediately concluded that for a sequence of this dissipative systems acting in fixed (unperturbed) time intervals, the norm of the final condition is smaller than that of the initial condition:

$$\|\delta Y_n\| = \left\| \left(\prod_{i=1}^{n} \Phi_i(t_i, t_{i-1}) \right) \delta Y_0 \right\| < \|\delta Y_0\| \tag{37}$$

This, in turn, means that the perturbations at each Poincaré section of (18) will decay at the next step and thus the periodic orbit is stable. This completes the proof of stability.

Corollary 1. *A system which is stable according to Theorem 1 is contractive in the sense of Lohmiller and Slotine (1998).*

Proof. It is immediately deduced from the fact that the Poincaré section utilized for the stability analysis is stroboscopic. That is, from any initial condition, the trajectories of the system converge to a single trajectory in time domain, i.e., the stable periodic orbit of the system.

Remark 1. Stability and contractivity ensure that the system, unlike some other piecewise linear systems such as in Schulman (1983), will not show chaotic behaviors. But more importantly, the contractive behavior guarantees that transitions between phases occur at predefined instants. This is a significant characteristic for locomotion control, so much so that the rest of our controller is built upon this. Again, note that we have exploited the hierarchical structure of (1) and designed the inner-most control loop to be contractive.

Remark 2. The single-support phase, as designed by (7) is passive and dissipative. Therefore, the energy lost due to damping is compensated exclusively during double-support phases.

Remark 3. In Theorem 1, we assumed that the sequence of {DS,SS,DS} is preserved. Since the cases in which the system is only in double-support are trivially stable (the system will not have a periodic orbit in single-support –see Remark 2), the only remaining case will be when the system goes to flight. Including the aerial phase results in numerous possible sequences of phases. Cham and Cutkosky (2007) considered various combinations of stance and flight in their hopping analysis. In our case, due to having two legs and one more phase (double-support), the number of cases that can happen will be much greater and we do not investigate them in the present work. However, intuitively, in the case of perturbation of the system into an aerial phase, since the system is purely energy-dissipative in single-support and because flight is energy-conservative, it is expected that the system gradually loses its energy by oscillating between stance and flight until it does not go to flight anymore and the results of Theorem 1 applies to it. Thus, in most cases, the basin of attraction of the oscillating system is expected to includes states corresponding to flight as well.

To investigate this, we simulated the system with the periodic orbit previously shown (Figure 7(a)) with an extreme initial condition (10 m height). Indeed, not only is the system stable and gradually goes to a normal sequence of single- and double-support (Figure 8(a)), but as Figure 8(b) shows, it is contractive and the two time trajectories (perturbed and unperturbed) gradually converge.

Remark 4. The case of overdamped systems (or underdamped in single-support and overdamped in double-support) can be proven similarly. As expected and as Figure 9 depicts for $\zeta_{ss} = 2$ and unchanged other parameters, the convergence becomes much faster compared to Figure 8. Whereas it takes about 15 seconds in the underdamped case for the trajectories to converge (Figure 8(b)), in the overdamped case, the convergence is decreased to less than 3 seconds (Figure 9(b)). Also note the "flatness" of the periodic orbit in the overdamped case as opposed to the oscillatory trajectory of the underdamped system. Therefore, for a fixed mass and spring stiffness, one can think of the selection of damping as a trade-off between efficiency of the system and its speed of convergence.

Having established the stability of the vertical oscillations, in the next subsection, we take advantage of the hierarchical structure of (1) and address the stability of the horizontal-plane motion.

3.3 Control of Horizontal-Plane Motion

As mentioned, ATRIAS is not equipped with yaw actuation, and thus it cannot actively steer. This fact together with assuming that the two-point contact feet prevent yaw motion (Assumption 2), leads to considering only walking in a

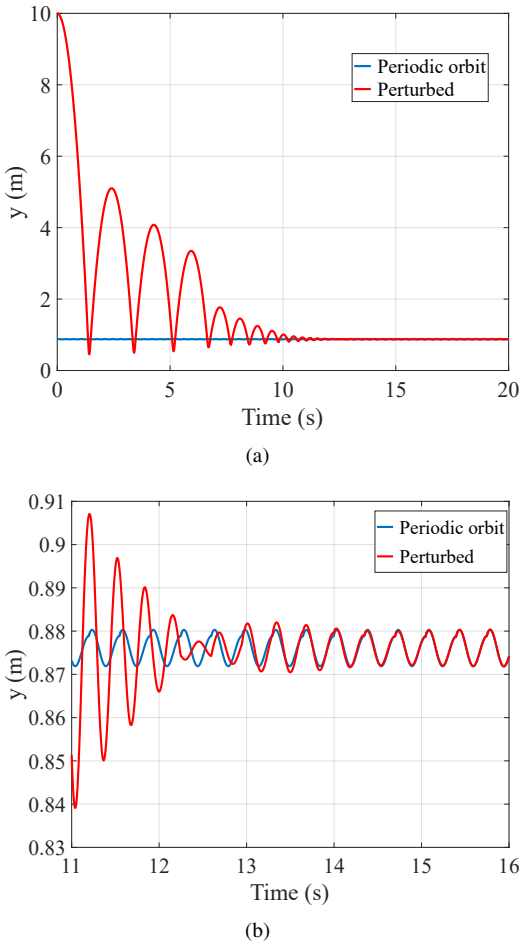

Figure 8. The extreme perturbation of the 1D vertical oscillator, starting from 10 m of height. (a) Response of the system compared with its periodic orbit. (b) Zoomed trajectories demonstrate contractivity.

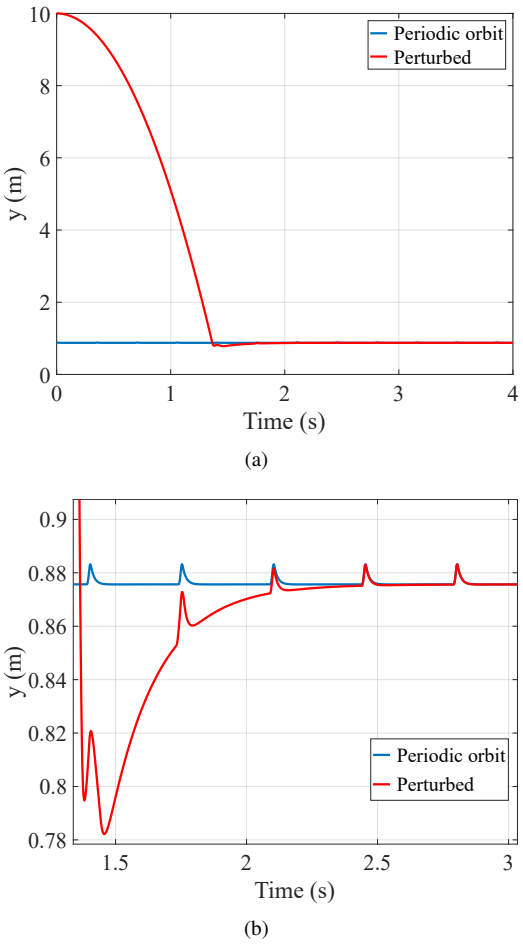

Figure 9. The extreme perturbation of the 1D vertical oscillator for an overdamped case. (a) Response of the system compared with its periodic orbit (b) Zoomed trajectories demonstrate contractivity.

straight line. Based on this and using Assumption 1, for the local analysis of stability (small changes in the velocity), the dynamics of the two axes become decoupled; similar controllers (with different set-points and parameters) can be used for x and z directions; and hence the analysis of the system can be performed in 2D.

The spring-mass model considered (Figure 4) has a single actuator in the leg length direction. Therefore, the stance force does not have a component in the leg angle direction. However, due to the massless legs, it is often assumed that during the swing phase, the touchdown angle can be controlled with zero control effort. We use this control input to control the velocity of the mass. Note that if we define the Poincaré section at the touchdown point, the Poincaré map will have the following form:

$$\begin{bmatrix} x_{i+1} \\ \dot{x}_{i+1} \end{bmatrix} = P_x \left(\begin{bmatrix} x_i \\ \dot{x}_i \end{bmatrix} \right) \tag{38}$$

where x is measured with respect to the touching-down foot as in Figure 4 and thus is reset in every step. Then controlling the velocity as a function of touchdown angle defines both the position and velocity components of the Poincaré section. In other words, (38) can be rewritten as:

$$\dot{x}_{i+1} = P_{\dot{x}}(\dot{x}_i) \tag{39}$$

Therefore, we only design our controller for the stability of (39). But before that, we prove a lemma about how $x(t)$ and $\dot{x}(t)$ vary with the change of the touchdown angle.

Lemma 1. *Assume that the bipedal version of the system described by* (1) *has a stable periodic orbit in the y direction described by* (10)-(12). *If x_0 denotes the touchdown position of the mass with respect to the foot (as in Figure 4), then for any touchdown speed $\dot{x}_0$ and any time t until the next touchdown, we have $\frac{\partial x(t)}{\partial x_0} \geq 1$ and $\frac{\partial \dot{x}(t)}{\partial x_0} \geq 0$.*

Proof. The x-axis dynamics in bipedal spring-mass model have the following form:

$$m\ddot{x} = F_{l,1}\frac{x}{y} + F_{l,2}\frac{d+x}{y} \tag{40}$$

where index 1 refers to the leg touching down, x is measured from the foot of this leg to the mass, and d is the location of the second foot with respect to the first foot, which will be fixed after touchdown. Note that (40) refers to both DS and SS phases where during SS, $F_{l,2} = 0$. A schematic of the system in DS phase is depicted in Figure 10.

Defining $t = 0$ at the touchdown instant, we have $\frac{\partial x(t)}{\partial x_0}\big|_{t=0} = 1$ and $\frac{\partial d}{\partial x_0} = -1$. Also, because at this stage the velocity of the mass at touchdown is not related to the

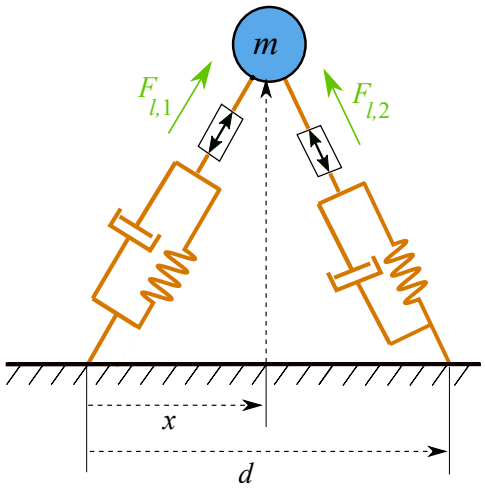

Figure 10. Bipedal spring-mass system in double support and its corresponding parameters. Note that both x and d can be positive or negative.

touchdown position, we have $\frac{\partial \dot{x}(t)}{\partial x_0}\big|_{t=0} = 0$. The change of acceleration with respect to x_0 can be obtained as:

$$m\frac{\partial \ddot{x}}{\partial x_0} = \frac{F_{l,1}}{y}\frac{\partial x}{\partial x_0} + \frac{F_{l,2}}{y}(-1 + \frac{\partial x}{\partial x_0}) \tag{41}$$

Note that $F_{l,i} \geq 0$ and $y > 0$ are independent of the x axis attributes and dynamics. Recalling that $F_{l,1}(0) = 0$ (touchdown) and $\frac{\partial x(t)}{\partial x_0}\big|_{t=0} = 1$, we have $\frac{\partial \ddot{x}}{\partial x_0}\big|_{t=0} = 0$. This means that, in order to determine the behavior of variations immediately after touchdown, we need to investigate the jerk. We have:

$$m\dddot{x} = \frac{\dot{F}_{l,1}}{y}x + F_{l,1}.\frac{\mathrm{d}}{\mathrm{d}t}(\frac{x}{y}) + (d+x).\frac{\mathrm{d}}{\mathrm{d}t}\left(\frac{F_{l,2}}{y}\right) + \frac{F_{l,2}}{y}\dot{x} \tag{42}$$

Similar to the case of acceleration, taking derivative with respect to x_0 and simplifying at $t = 0$ results in:

$$\frac{\partial \dddot{x}}{\partial x_0}\bigg|_{t=0} = \frac{\dot{F}_{l,1}(0)}{my(0)} > 0, \tag{43}$$

because the leg force is increasing at touchdown.

Equation (43) means that for some $t_p > 0$ and $\forall t \in (0, t_p]$, we have $\frac{\partial \dot{x}(t)}{\partial x_0} > 0$ and $\frac{\partial x(t)}{\partial x_0} > 1$. Assume that $t_x > t_p$ is the first instant when $\frac{\partial x(t)}{\partial x_0} = 1$. By the mean value and intermediate value theorems, there is a t_v such that $t_p < t_v < t_x$ and $\frac{\partial \dot{x}}{\partial x_0}\big|_{t=t_v} = 0$. Similarly, there will be a t_a with $t_p < t_a < t_v$ and $\frac{\partial \ddot{x}}{\partial x_0}\big|_{t=t_a} = 0$. However, since $\frac{\partial x(t)}{\partial x_0}\big|_{t=t_a} > 1$,

$$\begin{aligned} m\frac{\partial \ddot{x}}{\partial x_0}\big|_{t=t_a} &= \frac{F_{l,1}}{y}\frac{\partial x}{\partial x_0}\big|_{t=t_a} + \frac{F_{l,2}}{y}(-1 + \frac{\partial x}{\partial x_0}\big|_{t=t_a}) \\ &> \frac{F_{l,1}(t_a)}{y(t_a)} \\ &> 0 \end{aligned} \tag{44}$$

which is a contradiction. Therefore, we require to have $\frac{\partial x(t)}{\partial x_0} > 1$, $\frac{\partial \dot{x}(t)}{\partial x_0} > 0$, and $\frac{\partial \ddot{x}(t)}{\partial x_0} > 0$ for all $t > 0$ until the given set of dynamics changes (i.e., next touchdown). This completes the proof.

Next, we use the results of Lemma 1 to develop our foot placement control scheme. First, we stabilize the vertical oscillation in 2D (and equivalently, in 3D), i.e., when the desired horizontal velocity is zero, which we call "in-place walking", and then extend the results to non-zero horizontal speeds.

Theorem 2. *There is a class of functions in the form of $x_0 = \gamma(\dot{x}_0)$ which stabilize the system governed by (40) in the horizontal direction, and by (10)-(12) in the vertical direction, to $\dot{x} = 0$.*

Proof. By integrating (40) we obtain:

$$\dot{x}(T) - \dot{x}_0 = \int_0^T \left(\frac{F_{l,1}(t) + F_{l,2}(t)}{my(t)}x + \frac{F_{l,2}(t)}{my(t)}d\right)\mathrm{d}t \tag{45}$$

where T is the time at the next touchdown, which, due to the decoupled dynamics (see Proposition 1), depends only on the vertical-direction dynamics and is independent of horizontal foot placement. Again, note that $F_{l,2}$ will be zero once leg 2 goes to swing. We have:

$$\frac{\partial \dot{x}(T)}{\partial \dot{x}_0} - 1 = \int_0^T \left(\frac{F_{l,1} + F_{l,2}}{my}\frac{\partial x}{\partial \dot{x}_0} + \frac{F_{l,2}}{my}\frac{\partial d}{\partial \dot{x}_0}\right)\mathrm{d}t \tag{46}$$

Substituting

$$\begin{cases} \frac{\partial x}{\partial \dot{x}_0} = \gamma'(\dot{x}_0)\frac{\partial x}{\partial x_0} \\ \frac{\partial d}{\partial \dot{x}_0} = \gamma'(\dot{x}_0)\frac{\partial d}{\partial x_0} = -\gamma'(\dot{x}_0) \end{cases} \tag{47}$$

we obtain:

$$\frac{\partial \dot{x}(T)}{\partial \dot{x}_0} = 1 + \gamma'(\dot{x}_0)\int_0^T \left(\frac{F_{l,1} + F_{l,2}}{my}\frac{\partial x}{\partial x_0} - \frac{F_{l,2}}{my}\right)\mathrm{d}t \tag{48}$$

For stability we need to have:

$$-1 < \frac{\partial \dot{x}(T)}{\partial \dot{x}_0} < 1 \tag{49}$$

Now since by Lemma 1 $\frac{\partial x}{\partial x_0} \geq 1$, we have:

$$\int_0^T \left(\frac{F_{l,1}(t) + F_{l,2}(t)}{my(t)}\frac{\partial x}{\partial x_0} - \frac{F_{l,2}(t)}{my(t)}\right)\mathrm{d}t > 0 \tag{50}$$

Thus, in order to have $\frac{\partial \dot{x}(T)}{\partial \dot{x}_0} < 1$, it is necessary and sufficient to have:

$$\gamma'(\dot{x}_0) < 0 \tag{51}$$

Next, we investigate the second stability condition, i.e., $\frac{\partial \dot{x}(T)}{\partial \dot{x}_0} > -1$. For this condition, notice that $\frac{\partial x}{\partial x_0}$ in (48) cannot have a finite escape time. Otherwise, there will also be a finite escape time for $\frac{\partial \ddot{x}}{\partial x_0}$ in (41), which, due to boundedness of $F_{l,i}(t)/y(t)$ and by the comparison lemma is not possible. Therefore, a γ' sufficiently close to zero ensures that $\frac{\partial \dot{x}(T)}{\partial \dot{x}_0} > -1$, and thus the stability of the system.

Remark 5. Note that (48) is independent of the desired velocity. If $\gamma(0) = 0$, then Theorem 2 ensures that the system converges to a stable periodic orbit with $\dot{x} = 0$ (in-place walking). Convergence to periodic orbits with nonzero horizontal velocities ($\dot{x} \neq 0$) is possible simply by setting $\gamma(0) \neq 0$. The resultant periodic orbit is still stable, because, as mentioned, (48) is independent of the desired velocity. In such a case, one can use $\gamma = \gamma(\dot{x}_0, \dot{x}_d)$ for emphasis. In this form, we have $\gamma(0, 0) = 0$ and $\frac{\partial \gamma(\dot{x}_0, \dot{x}_d)}{\partial \dot{x}_0} < 0$. Note that the lower band on γ' may change based on the desired velocity.

Remark 6. Theorem 2 can be viewed as a generalization of Raibert's hopping foot placement controller (Raibert (1986)) to a wide class of functions, its extension to the bipedal spring-mass walking (as opposed to hopping), and its mathematical proof. His proposed linear scheme ($x_0 = -\dot{x}T/2 - k_{\dot{x}}(\dot{x} - \dot{x}_d)$), with a constant $\gamma' = -T/2 - k_{\dot{x}} < 0$, can be regarded as the simplest form of $\gamma(\dot{x}_0, \dot{x}_d)$ that satisfies the required conditions.

Remark 7. Because $\frac{\partial \ddot{x}(t)}{\partial x_0} > 0$, we can conclude that $\frac{\partial \dot{x}(t)}{\partial x_0}$ is monotonic and thus bijective. Therefore, there exists x_0 and t_c at which $\dot{x}(t_c) = 0$ and $x(t_c) = 0$. Similar to Pratt et al. (2006) and Koolen et al. (2012), this can be called the *capture point* of the spring-mass system, where in the absence of external perturbations, the system will remain vertical. Note that in general $t_c \neq T$.

Next, we formulate the spring-mass system with a torso and analyze its stabilization.

3.4 Torso Stabilization

Figure 3 displays the spring-mass system with a torso. In this case, the hip is equipped with a rotary actuator with the torque τ_h. Similar to Assumption 3 for the legs, we develop our controller under the following assumption:

Assumption 5. *If ϕ is the torso angle with respect to the vertical direction, then* $\sin\phi = \tan\phi = \phi$.

Theorem 3. *For every $\epsilon > 0$ there is a control law $\tau_{h,\epsilon}$ for the hip torque, which stabilizes the torso dynamics to the origin and does not affect the stability of the translational degrees of freedom per* (1).

Proof. Using Assumption 5, the dynamics of the torso can be written as:

$$I_t\ddot{\phi} = \tau_h.(1 + l_G/y) + F_l l_G.(\phi + x/y) - mgl_G\phi \quad (52)$$

We use a partial feedback linearization scheme (Spong (1994)) to stabilize the torso to $\phi = 0$ and $\dot{\phi} = 0$:

$$\tau_{h,\epsilon} = -F_l l_G \frac{\phi y + x}{y + l_G} - (k_{p,\phi}\phi + k_{d,\phi}\dot{\phi})\frac{y}{y + l_G} + \frac{mgl_G y\phi}{y + l_G} \quad (53)$$

Thereby,

$$I_t\ddot{\phi} + k_{d,\phi}\dot{\phi} + k_{p,\phi}\phi = 0 \quad (54)$$

which is exponentially stable.

Next, we investigate the effect of this controller on the translational degrees of freedom. We have:

$$\begin{cases} m\ddot{x} = \frac{x - \phi l_G}{y + l_G} F_l - \frac{k_{p,\phi}\phi + k_{d,\phi}\dot{\phi} - mg}{y + l_G} \\ m\ddot{y} = F_l(1 + l_G\frac{x}{y}(\frac{\phi y + x}{y + l_G})) \\ \qquad - mg(1 + \frac{l_G x\phi}{y(y + l_G)}) \\ \qquad - (k_{p,\phi}\phi + k_{d,\phi}\dot{\phi})\frac{x}{y(y + l_G)} \\ I_t\ddot{\phi} + k_{d,\phi}\dot{\phi} + k_{p,\phi}\phi = 0 \end{cases} \quad (55)$$

Similar to Poulakakis and Grizzle (2009), we rewrite the dynamics in the singular perturbation form (Khalil (1996)) by defining $[\tilde{\phi}_1 \quad \tilde{\phi}_2]^T = [\epsilon\phi \quad \dot{\phi}]^T$. Using this, and taking $k_{p,\phi} = \tilde{k}_{p,\phi}/\epsilon^2$ and $k_{d,\phi} = \tilde{k}_{d,\phi}/\epsilon$, the torso dynamics takes the following form:

$$\epsilon \begin{bmatrix} \dot{\tilde{\phi}}_1 \\ \dot{\tilde{\phi}}_2 \end{bmatrix} = \begin{bmatrix} 0 & 1 \\ -\tilde{k}_{p,\phi} & -\tilde{k}_{d,\phi} \end{bmatrix} \begin{bmatrix} \tilde{\phi}_1 \\ \tilde{\phi}_2 \end{bmatrix}, \quad (56)$$

which puts (55) in the standard singular perturbation form and converges to zero at a rate set by ϵ (see Poulakakis and Grizzle (2009) for further details). Thus, the slow translational dynamics can be rewritten with $\phi = 0$ and $\dot{\phi} = 0$ as follows:

$$\begin{cases} m\ddot{x} = \frac{x}{y + l_G} F_l \\ m\ddot{y} = F_l(1 + l_G\frac{x^2}{y^2(y + l_G)}) - mg \end{cases} \quad (57)$$

Noting that $x^2/y^2 = \theta^2 \approx 0$, we will have:

$$\begin{cases} m\ddot{x} = \frac{x}{y + l_G} F_l \\ m\ddot{y} = F_l - mg \end{cases} \quad (58)$$

which is exactly the same as (1), with a transformation $y \to y + l_G$ in the horizontal direction. In other words, if the torso control is fast enough, for small angles, it is sufficient to consider the CoM (rather than the hip) for the reference of the horizontal dynamics. This is expected, as in the point-mass case the CoM and the hip coincide. This concludes the proof.

Remark 8. For the sake of brevity, the formulation of the dynamics and control design in Theorem 3 was done for a planar case. However, using Assumptions 3 and 5 it is straightforward (albeit lengthy) to show that in 3D with two angular degrees of freedom for the torso (roll and pitch), similar partial feedback linearization and singular perturbation schemes lead to the same result.

Remark 9. In the case of off-center hips (as in Figure 3, back view, where there is a nonzero distance between the hips), it can be shown that (58) changes to

$$\begin{cases} m\ddot{x} = \frac{x}{l + l_G} F_l \\ m\ddot{y} = \frac{y + l_G}{l + l_G} F_l - mg \end{cases} \quad (59)$$

where l is the change in height due to hip offset when the leg is not vertical ($\theta \neq 0$) and it can be obtained from $l = y + \rho\sin(\pi/2 - \theta)$, where ρ is the hip offset from the

center. Since by Assumption 3, $\pi/2-\theta$ is small, l simplifies to $l = y + (\pi/2-\theta)\rho$. Taking $\pi/2-\theta$ approximately less than 0.1 rad, in the case of ATRIAS, $(\pi/2-\theta)\rho < 0.018$ m, which is much smaller than the leg length (2% for a 0.90-m leg length) and thus its effect is negligible. Based on this, we use (58) for the analysis of both sagittal and frontal planes of ATRIAS.

Remark 10. The possibility of a fast set of dynamics for torso stabilization is in accordance with design of ATRIAS and its precise and high-bandwidth torque-control series elastic actuators (Kemper et al. (2010); Hubicki et al. (2016)). However, the horizontal force required to transfer this torque to the torso (through redirection of the GRF) can only be present when there is a sufficiently high vertical force to satisfy the friction cone constraints. Therefore, especially at the beginning and end of the stance phase, applying large torso stabilization torque becomes infeasible. We briefly discuss implications of this problem in the next subsection.

3.5 Practical Considerations for the Controller

Although the controller has been designed to provide maximum stability, for the implementation on the robot, some practical modifications and considerations have to be applied. In this subsection, we list them and discuss their effects on the performance of the controller.

3.5.1 Time-Based Feedforward Trajectories and Pushoff

As discussed, the feedforward time-based trajectories in the leg length direction essentially create a forced-oscillation scheme, which leads to highly stable and robust oscillations. For the sake of simplicity of the solutions, we chose sine functions as the time-based inputs in §3.2. However, it is possible to use other periodic excitations, as they would still lead to a forced oscillation. We use this idea for two different goals, namely, pushoff and avoiding toe-stubbing.

The time-based trajectories can be altered to change the energy of the system. Note that, as mentioned, with the proposed functions in (5) and (6), during single-support, the actuators do not provide any energy to the system and the energy changes solely by the dissipation of the leg damper. Theoretically, the energy provided in double-support can stabilize the system in any case, but the forward speed associated with the resulted periodic orbits will be limited. Therefore, to increase the forward speed and inspired by the biological locomotion where the energy of the gait is provided by pushoff at the latest stage of the stance phase (see Zelik et al. (2014); Lipfert et al. (2014)), we use a similar idea for energy injection.

Despite the fact that in human walking, pushoff energy injection seems to have a more direct role in the swing initiation (Lipfert et al. (2014)), in our system, it can also be related to the forward velocity. Since at the end of stance the leg has its maximum forward angle, a greater leg force F_l at this stage causes greater horizontal acceleration and can increase the velocity directly. In contrast, pushoff at other stages of the stance phase, although will increase the energy, only can indirectly affect the velocity (later in the cycle, through foot placement choice). Based on these motivations, we rewrite the time-based trajectory for $l_{m,1}$ in (5) in the following form ($l_{m,2}$ can be written in a similar way):

$$l_{m,1}(t) = \begin{cases} l_0 & t_0 \le t < t_0 + t_{po} \\ l_0 + \Delta l_{po} & t_0 + t_{po} \le t < t_0 + \pi/\omega \\ l_0 + \Delta l_{sw} & t_0 + \pi/\omega \le t \le t_0 + 2\pi/\omega \end{cases} \tag{60}$$

where $t_0 = 2(i-1)\pi\omega$ is the start of the ith stride, t_{po} with $(2i-1/2)\pi\omega < t_{po} < (2i-1)\pi\omega$ is the pushoff start time, Δl_{po} is pushoff, and Δl_{sw} is the change in the second half of the time-based trajectory to maintain the C^1 continuity after the addition of pushoff. We propose the following scheme for pushoff:

$$\Delta l_{po} = k_{1,po}\dot{x}_d + k_{2,po}(\dot{x}_d - \dot{x}) \tag{61}$$

which means that as the desired speed and the error in the speed tracking increase, the pushoff also increases. Note that the presented pushoff scheme increases both horizontal and vertical velocities. The foot placement control then regulates the distribution of the energy between vertical and horizontal motions through an appropriate touchdown angle.

In contrast with the second half of the feedforward trajectory (which was used for pushoff and energy regulation), the first half can be altered to avoid toe-stubbing. The symmetric nature of the sine function causes the maximum leg retraction to happen in the middle of the swing. It may be desired to shift the maximum retraction to an earlier phase to reduce the chance of toe-stubbing. Again, note that unlike hopping and running (where the upward motion of the body lifts the leg off the ground), the leg has to be retracted actively for starting the swing phase in the case of walking.

3.5.2 Discrete PD Controller for Foot Placement

The expression we start with for $\gamma(\dot{x}_0, \dot{x}_d)$ as our foot placement scheme has the following simple form:

$$x_0 = \gamma(\dot{x}_0, \dot{x}_d) = \bar{\gamma}_0(\dot{x}_d) - \bar{k}_{p,f}\dot{x} \tag{62}$$

where $\frac{\partial \bar{\gamma}_0}{\partial \dot{x}_d} < 0$ and $\bar{\gamma}_0$ can be tuned using simulation or experimental results. Similar to the more basic form of Raibert (1986), (62) can be rewritten as

$$x_0 = \gamma(\dot{x}_0, \dot{x}_d) = \gamma_0(\dot{x}_d) - k_{p,f}(\dot{x}_0 - \dot{x}_d) \tag{63}$$

Notice that (63) has the form of a discrete proportional controller with a feedforward term (γ_0). Although this form was proven to stabilize the system (Theorem 2), we found that its extension to a discrete PD can make the operation of the robot smoother, especially for overcoming velocity perturbations (stabilization against pushing, for example). The discrete PD control will have the following form:

$$x_0 = \gamma_0(\dot{x}_d) - k_{p,f}(\dot{x} - \dot{x}_d) - \frac{\pi}{\omega}k_{d,f}(\dot{x} - \dot{x}_{-1}) \tag{64}$$

where $\dot{x}_{-1}$ represents the touchdown speed at the previous step and typically $k_{d,f} \ll k_{p,f}$.

We also examined the idea of adding an integral term to extend the foot placement scheme to a discrete PID controller, with the goal of minimizing the steady state error between $\dot{x}_0$ and $\dot{x}_d$ (see Remark 5). However, the integral

term did not demonstrate any significant improvement with small integral gains and it resulted in instability with larger gains. Hence, we used the discrete PD for our experiments.

3.5.3 Torso Control, Friction Cones, and Leg Swing In order to avoid the violation of friction-cone constraints and foot-slipping (which may occur during stance phase as a result of inadequate static friction), we need to apply constraints to the torso controller. We do this by limiting the leg angle torque based on the leg force. In other words, if the measured leg force is not sufficiently high, then the leg angle torque will be limited by the maximum of the static friction force. The maximum friction is estimated based on the friction coefficient and the vertical force (measured from the spring deflection and the Jacobian of the leg mechanism). Furthermore, note that the switching between stance and swing is generally not aligned with the transition of the feedforward trajectories, especially when the robot undergoes perturbations. This is especially important for the leg angle torques, because of their different role in stance and swing phases (torso control versus swinging the leg). Therefore, in order to achieve a smooth transition between these two tasks, we define a pair of fuzzy sets and associated membership functions (one for each leg) for differentiating between stance and swing phases. For the stance phase we define:

$$\mathcal{U}_{st} := \left\{ \big(F_y, \mu_{st}(F_y)\big) | \mu_{st}(F_y) \mapsto [0,1] \right\} \tag{65}$$

with

$$\mu_{st}(F_y) = \begin{cases} 0 & F_y < f_1 \\ \frac{F_y - f_1}{f_2 - f_1} & f_1 \le F_y < f_2 \\ 1 & F_y \ge f_2 \end{cases} \tag{66}$$

where F_y is the vertical leg force and f_1 and f_2 are tunable parameters. Thereby, the leg angle torque τ_h at each moment is computed from

$$\tau_h = \mu_{st}\tau_{h,\epsilon} + (1-\mu_{st})\tau_{h,sw}, \tag{67}$$

where $\tau_{h,sw}$ is the swing phase leg angle torque, which is obtained from a simple PD controller:

$$\tau_{h,sw} = k_p(\theta_d - \theta) + k_d(\dot{\theta}_d - \dot{\theta}) \tag{68}$$

and the desired leg angle is computed from the foot placement strategy (Theorem 2):

$$\theta_d = \pi - \cot^{-1}\big(-\gamma(\dot{x})/y\big) \tag{69}$$

Note that the foot placement is only used at the very end of the swing phase. Before that, we use a third order spline for θ_d, with initial condition set when μ_{st} becomes zero, and final conditions from $\pi + \tan^{-1}\gamma(\dot{x})$ and its time derivative. The duration of the spline is tunable and we took it as $0.75\pi/\omega$ after $\mu_{st} = 0$.

In addition to the torso angle control, foot slipping is also important for the calculation of the forward velocity $\dot{x}$. Specifically, because we used a forward kinematic analysis from the foot (as a point fixed to the ground) to the CoM to compute $\dot{x}$, the calculation is sensitive to foot slipping. Therefore, we used the same fuzzy set and membership function as in (65) and (66) for the selection of the leg based on which the velocity is computed:

$$\dot{x} = \mu_{st,\text{leg1}}\dot{x}_{\text{leg1}} + \mu_{st,\text{leg2}}\dot{x}_{\text{leg2}} \tag{70}$$

where $\dot{x}_{\text{leg1}}$ and $\dot{x}_{\text{leg2}}$ refer to the calculation of the CoM velocity based on the corresponding legs.

3.6 Reflex-Based Control of Walking on Uneven Ground

From the proofs presented for the design of different parts of the controller, one can conclude that the part most prone to instability is the torso stabilization. Vertical oscillations and horizontal foot placement paradigms can stabilize the spring-mass system (without torso) from a wide range of initial conditions. In contrast, the torso stabilization largely depends on the positioning of the foot on the ground and a sufficient level of GRF. Such destabilizing conditions usually do not happen in flat-ground walking, but they are the main reason of instability during step-downs. Specifically, during the stride after a step-down, the extra energy that the robot has gained can move it upward and lift the foot off the ground. This turns the torso control off (cf. (67)), which will result in the falling of the robot.

ATRIAS is not equipped with a vision system and thus cannot use vision and path planning to manage large changes in the terrain height. However, inspired by the remarkable ability of animals to negotiate highly uneven terrains without visual feedback (see Daley and Biewener (2006), for example), we seek a reflex-based control that stabilizes the system once a step-down occurs. Neural reflexes based on proprioceptive sensing are known to have an important role in robust locomotion of animals in uncertain environments (Jindrich and Full (2002); Borgmann et al. (2009); Proctor and Holmes (2010)). In what follows, we develop a stabilizing scheme for step-downs using the proprioceptive information of the robot's sensors.

As mentioned, the main problem arising during a step-down is the loss of control over the torso angle, which is an indirect consequence of the extra energy gained by the robot. Although, during step-downs the double-support phase is often eliminated (which, as discussed, is the energy-providing part of the gait), the natural energy dissipation of the robot is still not sufficient for larger step-downs. The intuitive solution for this problem is simple: dissipate the extra energy through flexing the leg. Note that before conversion to kinetic energy, the gravitational potential energy lost during step-down converts to elastic potential energy of the spring. Therefore, monitoring the spring deflection is the fastest proprioceptive detector of when something "irregular" happens.

Dissipation of the spring energy is done through retraction of the motors in leg length direction. Thereby, the spring force $F_{l,spring} = k(l_m - l)$ decreases as a result of the reduction of l_m. Moreover, since $F_{l,spring} = k(l_m - l) > 0$ (otherwise the leg is not on the ground) and at the same time $\dot{l}_m < 0$, the actuator power will be negative, which means the actuator absorbs the extra energy.

We use a simple threshold for the spring force magnitude. In this way, for example for leg 1, the feedforward trajectory of (5) changes to:

$$l_{m,td} = \min\{l_{m,1}, l_1 + \delta_{td}\} \tag{71}$$

where δ_{td} is a tunable constant and for our experiments with ATRIAS we chose it as 0.13 m.

Interestingly, the same idea can be used in the case of a step-up. If the swing leg continues its extension after it hits an obstacle, it will generate a strong backward force which will cause the robot not to climb the obstacle. Therefore, similar to step-downs, in such a situation, we retract the forward leg so that the back leg can push the robot up the obstacle. Once on the obstacle, the forward leg will start extending back and providing energy in order to restore the motion of the robot back to its stable periodic orbit.

4 Implementation and Results

In this section, we present the results of the implementation of the designed controller on ATRIAS. Hardware and software systems of the robot, experimental protocol, high-level descriptions of the results, and the qualitative relationship between the observed behavior of the robot and its design philosophy (i.e., realization of the spring-mass template) have been presented in our magazine article (Hubicki et al. (2018)) and are not repeated here. In contrast, in this paper, we quantitatively present and analyze the results to show the performance of the controller and its attributes.

4.1 Selection of the Controller Parameters

In general, we performed the selection and tuning of each of the controller parameters in two stages: simulation and experiment. The simulation environment used was a high-fidelity MATLAB-SimMechanics model of ATRIAS developed at Carnegie-Melon University (see Martin et al. (2015)). With the initial values from the simulation, the controller parameters were fine-tuned and finalized through experiments on the physical robot. In what follows, we present the main control parameters and the ideas and challenges associated with their selection.

4.1.1 Amplitude and Period of the Feedforward Oscillations As discussed in §3.2.2, the feedforward amplitude a determines the duration of double-support based on the energy dissipated in the single-support phase. Its tuning was primarily based on obtaining a natural-looking walk, as we did not find its effect on the stability of walking considerable. The default value used for a for flat-terrain walking was 0.20 m. For blind walking over obstacles (since the footsteps are not planned) and in order to avoid toe-stubbing during step-ups, a was increased to 0.30 m, which was equal to $\frac{1}{3}l_0$.

Unlike the amplitude, the period of the oscillations proved to have a strong effect on the stability of the robot. In particular, with a small ω, the robot would quickly fall laterally. It was observed that the same (small) frequency that stabilized the system in 2D (robot fixed to a boom mechanism –see DRL (2015i)), would not lead to stable in-place walking in 3D. The important difference for frontal actuators is that they have to move the sagittal-plane actuators along with the leg as they are in series with each other (Figure 2 –also see Rezazadeh et al. (2015)). This is an extra mass that makes the system deviate from Assumption 1 for the frontal motion. In order to overcome this problem, we increased the frequency until the system exhibited stable in-place walking at $\omega = 2\pi/0.7$ rad/s.

4.1.2 Joint Control Parameters With the proposed controller, joint control in both leg length and leg angle directions is based on position control, which is performed through current control of the motors. In the leg length direction, l_m defines the desired actuator position both in stance and swing. In the leg angle direction and during the swing, the desired leg angle θ_d (obtained from a spline function together with the foot placement scheme –see §3.5.3) determines the desired position of the motor. Also, during stance phase, the desired joint torque for torso stabilization can be translated to the desired position of the motor, according to the standard properties of the SEAs. Based on this, we used simple PD controllers for the joint position control.

The minimum stiffness that could be used for the leaf springs of ATRIAS was 2950 Nm/rad. With a smaller stiffnesses, the large deflection of the spring at high speeds would interfere with the robot's mechanism structure. With these springs, the equivalent stiffness in the leg length direction (about 25 kN/m, as obtained from the leg mechanism's Jacobian –see Rezazadeh et al. (2018)) proved to be too high for normal walking. Therefore, in order to provide more compliance to the system, we decreased the gains of the joint PD controllers. This allows the motors to move back under load and essentially act similar to an (open-loop) impedance (see Hogan (1985) for the theory, and Rezazadeh and Gregg (2016) and Elery et al. (2018) for the application ideas). Moreover, the motion of the motor during single support (in which, according to (5) and (6), the motor's desired position is fixed) causes the transmission system to dissipate more energy due to damping. This acts as an additional damper, which, as shown in Theorem 1, is vital for determining the characteristics of the oscillations of the system and its speed of convergence. The P and D gains of the PD controller were chosen as 3000 Nm/rad and 150 N.m.s/rad, respectively. The low P gain reduces the resultant leg stiffness to about 12 kN/m, which is very close to the leg stiffness of the humans when walking (see Farley and Ferris (1998)).

4.2 Experimental Results

The controller designed in the previous section was implemented on ATRIAS using Simulink Real-Time and was tested for a variety of tasks. The controller was capable of walking at different speeds, both in forward and backward directions. The desired speed was commanded to the robot computer using Wi-Fi and a PlayStation 3 controller.

Designing the controller based on Assumption 1 enabled the robot to walk backward and forward as well as sidestep (DRL (2015g)). Moreover, the robustness of the robot was successfully tested with a variety of perturbations, including walking on different terrains DRL (2015a), getting kicked DRL (2015e), a dodgeball barrage DRL (2015d), and walking on uneven ground DRL (2015h,c).

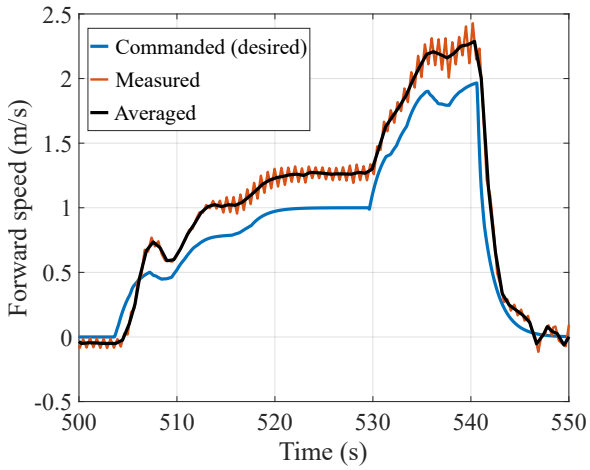

Figure 11. Forward speed during a walking test with ATRIAS. "Averaged" refers to the average speed during one stride.

Figure 12. A snapshot of the robot walking/running at 2.2 m/s.

In this subsection, we present the results of the two experiments that best represent the main characteristics of the designed controller: 1) continuous changing of walking speed until the maximum speed, and 2) walking on uneven terrains.

4.2.1 Experiment 1: High Speed Walking/Running Figure 11 depicts the desired and measured speeds for a 50-second walking test with ATRIAS. The robot starts from rest (in-place walking), then the desired speed is gradually increased to 1 m/s, then to 2 m/s, and finally back to zero speed. A snapshot of the trial can be seen in Figure 12. Also, the video of this experiment is available in DRL (2015f).

As Figure 11 shows, for a nonzero desired velocity, there is approximately a 0.2 m/s steady-state error in velocity tracking, which, as explained in the previous section, originates from the model error and the tuning of γ_0. Nevertheless, the robot was able to follow the same trend as the commanded signal and stop in a stable way at the end of the line.

Figure 13 displays the feedforward time-based trajectory $l_{m,1}$ (desired motor position), measured motor position, and measured leg length. Note that since the proportional gain of the motor's PD control was set almost equal to the spring stiffness, the motor position lies almost half-way between leg length and desired position. Also, note that the pushoff at the end of stance is nonexistent in zero speed and as speed increases, pushoffs also become greater. The tracking error in the second half of the swing phase is due to speed limitation of the motors.

Note that the period of the measured signals in Figure 13 perfectly matches that of the feedforward signal (0.7 s). This is more apparent in the time between the Poincaré sections (touchdown), which can be obtained from the GRF plots (Figure 14). As shown, at all speeds, the touchdown moments occur with the same period as the feedforward trajectory (± 0.001 s). Moreover, as the speed increases, the double-support time decreases, and for the speed of 2.2 m/s, there is an aerial phase instead of double-support, which means the robot has switched from walking to running. The right and left GRFs tend to become asymmetric as the speed increases, which presumably happens because the effect of asymmetries in the dynamical parameters of the system becomes stronger at greater speed. This is also visible in the actuator torque plots (Figures 15 and 16), where at 2.2 m/s, actuator 2 of the right leg applies higher torque than that of the left leg during stance. Note that the torques limit applied (in the software) is 600 Nm.

The high-speed asymmetry is not seen in the leg angle trajectories (Figure 17). The left and right legs maintain almost perfectly symmetric periodic orbits with the frequency of the forced oscillations ($2\pi/0.7$ rad/s). Naturally, as speed increases, the range of the sagittal plane leg angles also increases to provide greater stride lengths. This makes the system deviate from Assumption 3, but note that even at 2.2 m/s (Figure 17(c)), $\theta_{\max} = 2.09$ rad, for which the relative error for $\pi/2 - \theta - \cos(\theta)$ is still less than 5%. The sagittal-plane leg angle for in-place walking and the frontal leg angle during all trials remained well below 0.1 rad with respect to the vertical direction.

Torso angles throughout the experiment are depicted in Figure 18. As the speed increases, there is no visible change in the roll angle (frontal plane), but the ranges of oscillations for pitch, and especially for yaw, increase noticeably. Although the range of the pitch angle is greater at high speed due to larger leg forces F_l, it still remains less than 0.1 rad, which is in agreement with Assumption 5. However, the small feet of ATRIAS cannot constrain the yaw motion of the robot (Assumption 2) against these larger-magnitude forces at high speeds and the dynamical asymmetry of forces (Figure 14(c)) results in a slow rotation of the robot in one direction. This violation of the yaw constraint was the main obstacle for reaching greater walking speeds. Figure 19 presents a trial where the robot reached a speed of 2.5 m/s, but could not maintain this speed and the operator had to quickly stop the robot. The video of this experiment can be seen in DRL (2015b).

4.2.2 Experiment 2: Stable Walking on Uneven Ground Figure 20(a) displays the commanded and measured velocities during an experiment in which the robot, using the proposed reflex-based controller, stepped up and down a 15-cm obstacle for 11 consecutive passes without failure. The operator only corrected the direction of the robot (due to

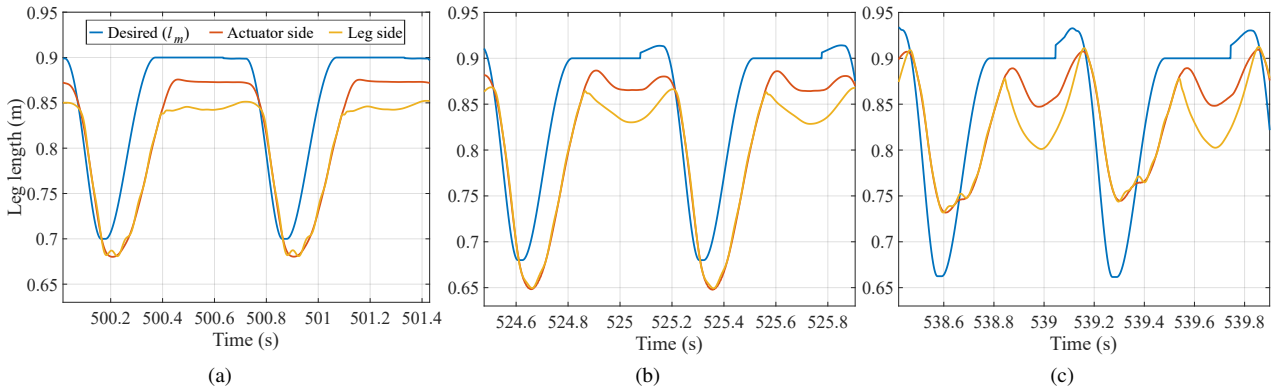

Figure 13. Desired (feedforward) neutral leg length trajectory for the right leg ($l_{m,1}$) compared with leg length and actuator leg length for two representative strides and three different speeds: (a) zero (in-place walking), (b) 1.25 m/s, and (c) 2.2 m/s.

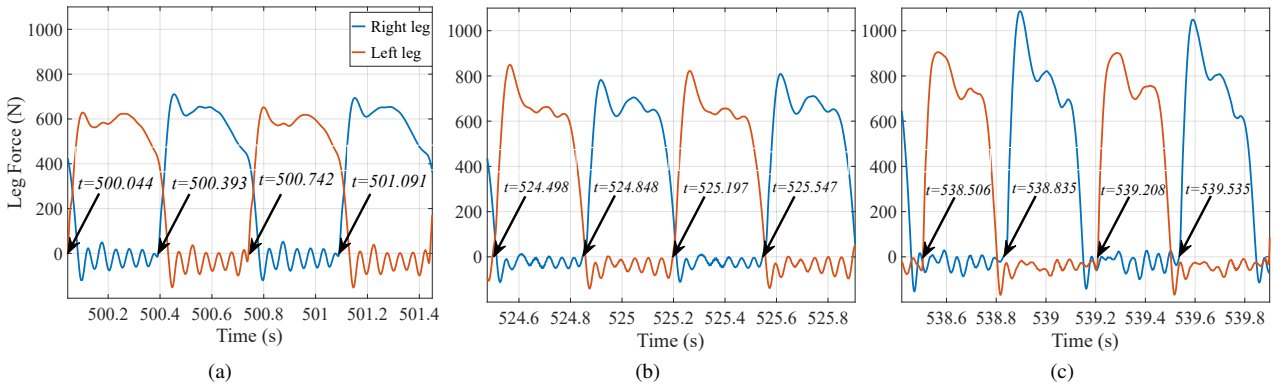

Figure 14. GRF during two representative strides for three different walking speeds: (a) zero (in-place walking), (b) 1.25 m/s, and (c) 2.2 m/s. The time instants show the moments of touchdown.

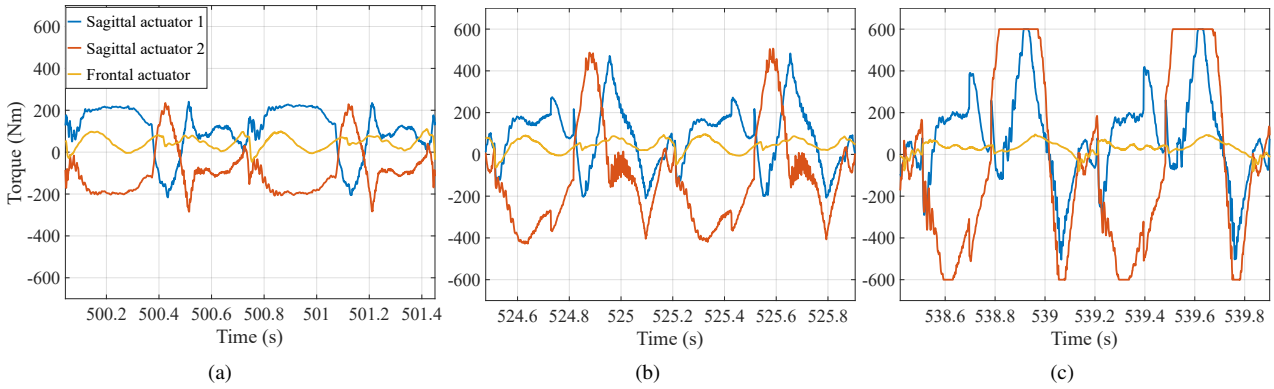

Figure 15. Actuator torque command (transmission output) of the right leg during two representative strides for three speeds: (a) zero (in-place walking), (b) 1.25 m/s, and (c) 2.2 m/s.

yaw rotation) after each pass. Figure 21(a) shows snapshots of a representative step-down. The flexion of the knee for absorbing the extra energy is noticeable in the left picture. The video of the experiment can be seen in DRL (2015c).

Figure 20(b) displays the leg forces during a representative pass over this obstacle. The step-up can be detected from the extended double-support phase caused by the early touchdown. Notice that the first peak of the double-peak profile of the leg (immediately after hitting the obstacle) is smaller than those of the previous and subsequent steps. This takes place because of the leg retraction due to the reflex-based control of (71), which can be seen in Figure 20(c). Moreover, in the case of step-up, the controller decreases the touchdown leg's desired leg length l_m immediately after touchdown and then gradually increases the leg length throughout the stance phase. Similarly, after sensing the step-down and the increased leg force as a result of it, pushoff is immediately stopped and the desired leg length is decreased, which in turn, quickly reduces the leg force.

We also used the same reflex-based controller for high-speed walking over a random obstacle-course with up to 10 cm of step-ups and step-downs (Figure 21(b)). As Figure 22 shows, the robot was able to reach a speeds of about 1.7 to 1.8 m/s in both direction. This had proven to be not possible

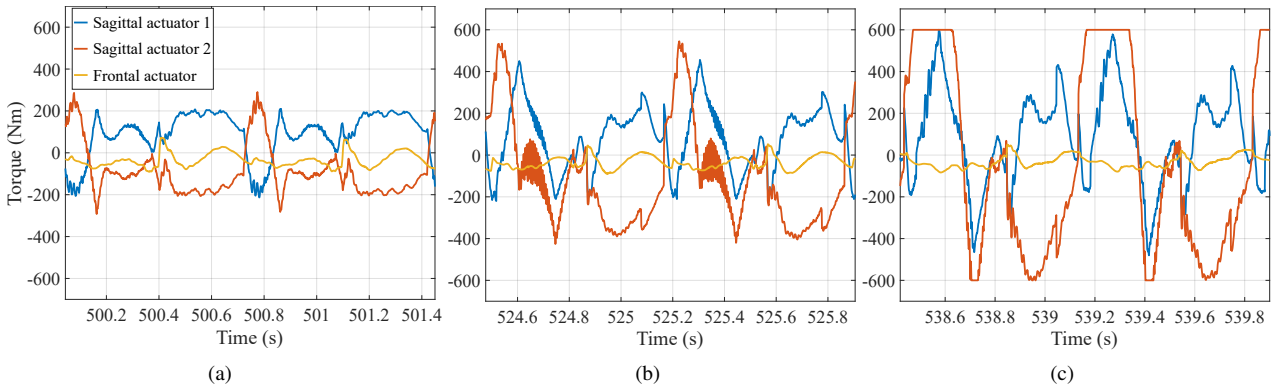

Figure 16. Actuator torque command (transmission output) of the left leg during two representative strides for three speeds: (a) zero (in-place walking), (b) 1.25 m/s, and (c) 2.2 m/s.

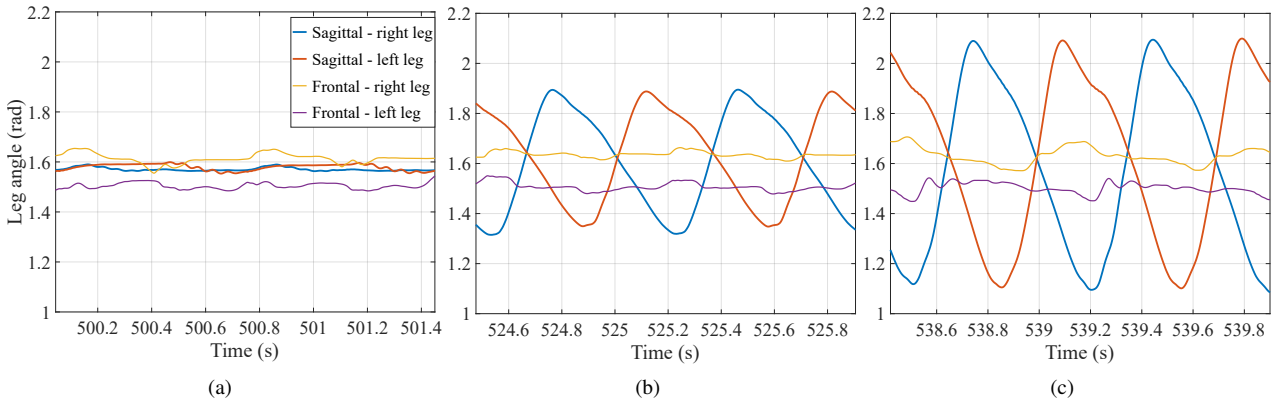

Figure 17. Evolution of sagittal- and frontal- plane leg angles during two representative strides for three speeds: (a) zero (in-place walking), (b) 1.25 m/s, and (c) 2.2 m/s.

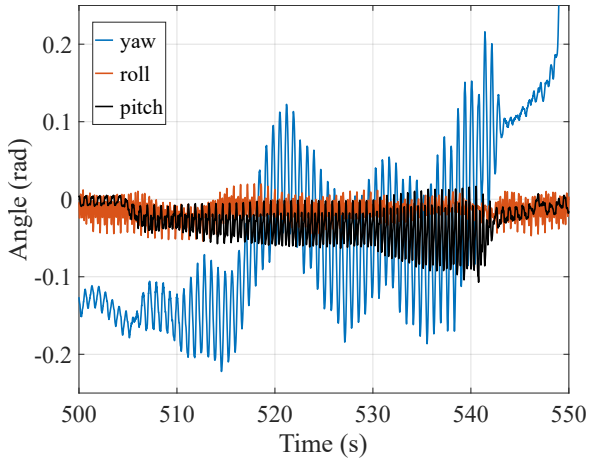

Figure 18. Evolution of Torso angles during the 50-second multi-speed trial. The rapid change of yaw angle at the end of trial is due to the operator's interference.

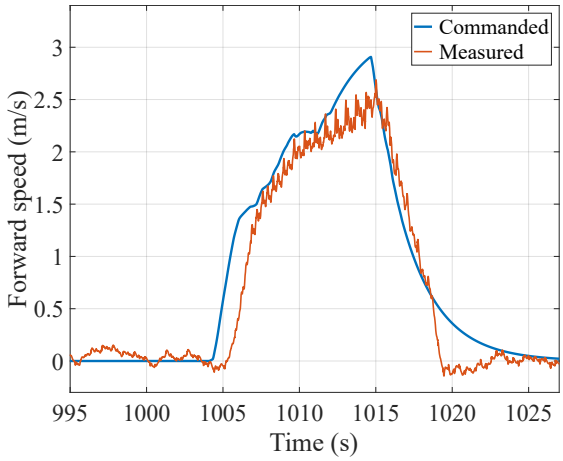

Figure 19. The desired and measured forward speed of the robot during a high-speed trial. The operator had to stop the robot at 2.5 m/s.

with the base controller without the addition of the reflex-based scheme, and the robot was limited to speeds of less than 1 m/s on such a course. The video of this trial can be seen in DRL (2015h).

5 Discussion and Conclusion

5.1 Advantages and Contributions

5.1.1 Theory The elegant three-part structure of Raibert's hopping controller (Raibert (1986)) based on decoupling vertical oscillations, foot placement, and torso angle regulation, despite its intuitiveness and popularity, was scarcely investigated through analytical proofs. In this work,

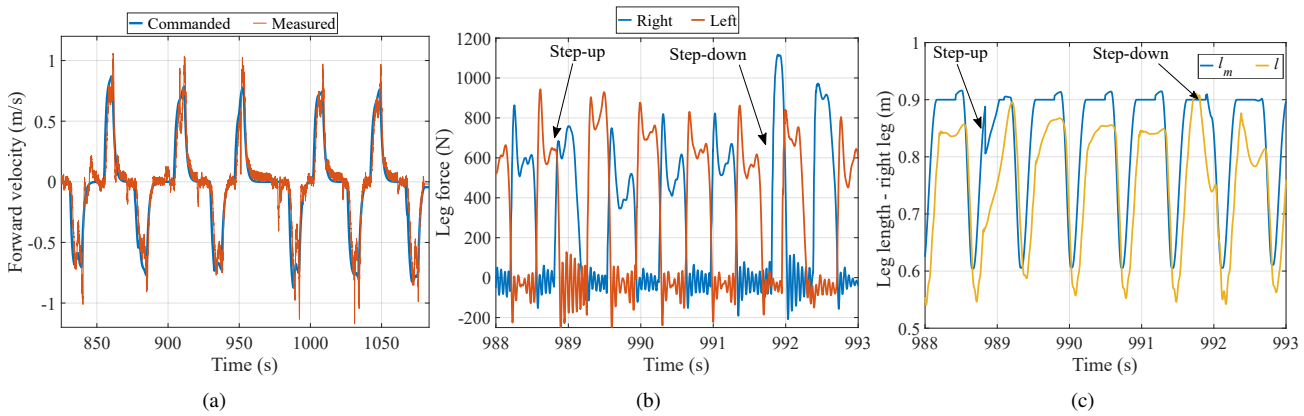

Figure 20. (a) The desired and measured forward velocities of the robot during 11 consecutive passes over a 15-cm obstacle. Negative velocities correspond to backward walking. (b) Leg forces during a representative pass over the 15-cm obstacle. The extended double-support phase indicates step-up (right leg touching the obstacle). A few strides later, the step-down can be detected from an aerial phase followed by a large force spike. (c) The reflex-based uneven-ground controller flexes the knee immediately after step-up and step-down in order to reduce the leg force.

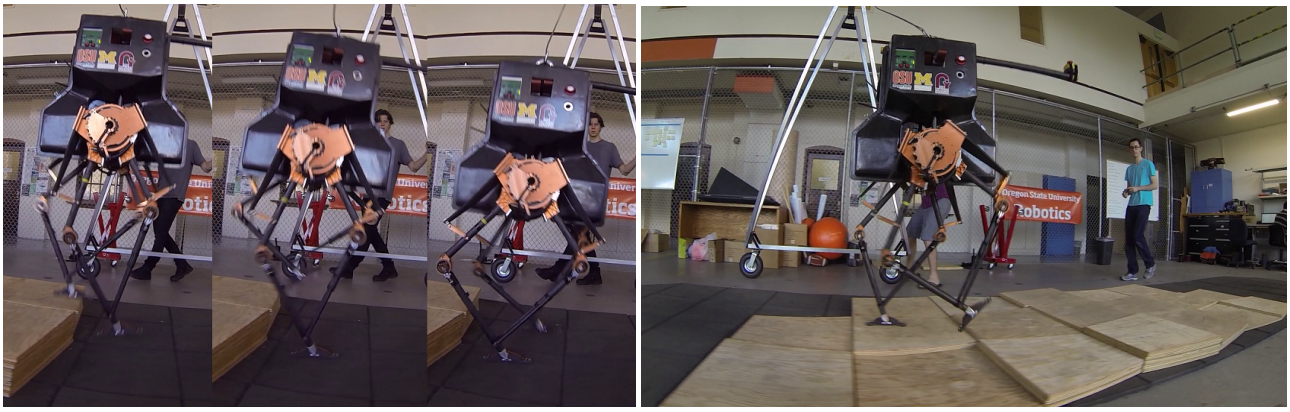

Figure 21. (a) Snapshots of a 15-cm step-down trial. The reflex-based controller flexes the knee after step-down in order to dissipate the gained energy. (b) A snapshot of the robot walking on a random obstacle-course with up to 10 cm of step-ups and step-downs.

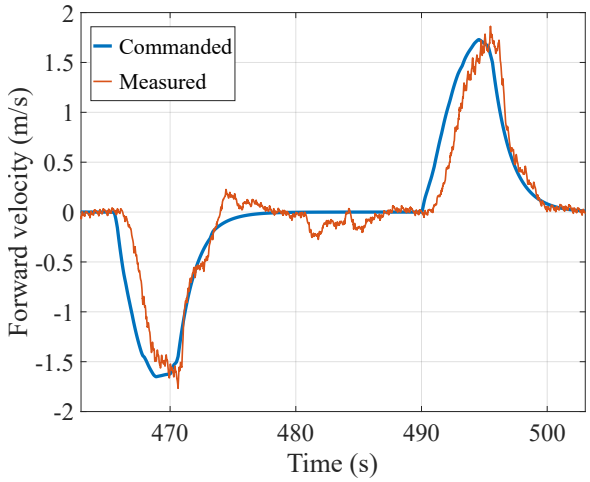

Figure 22. Velocity of the robot during a pair of forward and backward passes on the obstacle course.

using the widely-used Geyer's approximation (Geyer et al. (2005)), we showed that the spring-mass dynamics can be written in a hierarchical structure, which decouples the stability of the Poincaré section. As we showed, this facilitates control design and stability analysis of the system.

Another contribution of this work was introducing a time-based feedforward trajectory for spring-mass walking and its stability analysis. Clock-driven feedforward signals have been popular in the past two decades, but have been limited to hopping and running spring-mass systems. In this work, we designed a feedforward periodic excitation for control of vertical motion, which not only leads to a walking-like scheme (leg retraction, extension, stance), but also exhibits strong stability/contractivity characteristics. Since the vertical direction is the inner-most control loop in our hierarchical structure, its strongly stable characteristics are very important for control design for other DoFs and for the stability of the whole system.

The control of horizontal motion of the robot was performed through (discrete) foot placement. We obtained a class of functions that stabilize the spring-mass system (monopod or biped) with the proposed hierarchical dynamics. Then we showed that in the simplest case, the Raibert foot placement (Raibert (1986)) emerges from this

class of functions. Although not investigated in this work, the wide set of choices that Theorem 2 provides can be very useful in further developments based on this work. Moreover, Raibert's foot placement was hardly investigated in the literature for any reduced-order model in a rigorous analytical way. The closest attempt has been perhaps the work of De and Koditschek (2015), in which using assumptions such as neglecting gravity and assuming a fixed stance time and a fixed angular velocity (in addition to our assumptions), Raibert's foot placement was proven for a rigid inverted pendulum.

The hierarchical dynamics structure also allowed us to decouple the torso stabilization through feedback linearization and singular perturbation theory. The singular perturbation scheme can easily result in unrealistic controllers due to its demand for a fast set of dynamics. However, as shown in the experiments, in the presented paradigm, the singular-perturbation-based decoupling of the torso control works as expected and keeps the torso angles within an acceptable range, even at high speeds.

5.1.2 Results As confirmed by the experiments, the proposed controller consistently results in stable and periodic locomotion. The period is always enforced by the feedforward time-based trajectories, although due to asymmetries in dynamics, especially in high speeds, the resulted gait may be period-2.

The proposed controller was able to successfully accomplish the required task of stable and robust walking. At 2.2 m/s, ATRIAS with the proposed controller is one of the fastest untethered 3D bipeds in the world, perhaps with the exception of Boston Dynamics' new ATLAS. Indeed, the role of the controller is vital for achieving stable locomotion at such a speed. In comparison, ATRIAS with controllers presented in Griffin and Grizzle (2017) and Da and Grizzle (2019) (even though, as mentioned, partially adopted the structure presented in Rezazadeh et al. (2015)), did not exceed 1 m/s and 0.8 m/s, respectively. The main limiting factor for achieving higher speeds for our controller was the yaw oscillations that could not be constrained with ATRIAS's small feet. This finding was used in the design of ATRIAS's descendant, Cassie, which was designed with a yaw actuator for each leg for active control of this DoF.

The controller is based on a forced-oscillation scheme, and thus it has greater flexibility for minor changes and improvements compared to methods relying on periodic orbits found through optimization, such as HZD. An example of this was seen in §3.5.1, where the feedforward trajectory was changed to avoid toe-stubbing during swing phase and to add pushoff during stance phase. In addition, the framework can potentially make the use of learning and optimization algorithms easier, as Da and Grizzle (2019) have addressed.

Another advantage of the controller is that it requires minimal sensor information. Most of the control is done proprioceptively and is minimally affected by the noise. This is very useful for legged-robot applications, where impact and other noise sources tend to destabilize the system. In this regard, the fact that the heart of the controller is a time-based scheme is of great importance, as time can always be measured with effectively no error.

With this philosophy, we extended the controller to uneven-ground walking based on a proprioceptive reflex-based paradigm. Step-ups and step-downs were detected using the spring force, rather than using the long kinematic chain between the feet. In this way, the robot was able to blindly manage successive step-ups and step-downs on a 15-cm obstacle with no failure. To our knowledge, no other bipedal robot has been able to blindly walk over such obstacle in 3D. One can compare this result with the work by Park et al. (2013) in 2D with MABEL, in which they achieved a 12.5-cm step-up and a 18.5-cm step-down.

5.2 Limitations

The controller was designed based on the dynamics of a rigid-body torso with two compliant legs. Therefore, its success very much depends on the closeness of the dynamics of the robot to this reduced-order system. ATRIAS is a prime example of a design based on the spring-mass model (Hubicki et al. (2016)) and thus it made for a great platform for the proposed controller. However, as we observed, features of the robot that deviate from the ideal model (such as the extra mass on the frontal-plane actuators) can limit the performance of the controller. Nevertheless, a simulation study of applying the controller to humanoid robots with rigid joints and non-negligible leg masses showed that the extension to more general cases may be possible (Rezazadeh and Gregg (2016)). The work by Kim et al. (2016) on the whole-body control of a robot with point-feet and leg elasticity based on its reduced-order model is another interesting example that can be motivating for such an extension.

Assumptions 2 and 5 essentially enforce an upright and forward-facing torso at all times. This is acceptable for walking in a straight line, but for more extreme torso maneuvers and for steering on a non-straight path (most likely through yaw actuation), the controller needs to be extended and perhaps reformulated.

For achieving exactly a desired speed, γ_0 in Theorem 2 has to be chosen very accurately. In practice, there will always be an error, no matter how exact the formulation of the system's dynamics and its parameters are. We tried adding a discrete integral term to the foot placement control in order to reduce this error, but it did not prove to be effective. Perhaps an inner-loop controller for actively choosing γ_o based on the velocity tracking error can lead to the reduction of this error.

Acknowledgements

This work was not possible without the help from Oregon State University (Andy Abate, Ryan Domres, Christian Hubicki, Mikhail Jones, Andrew Peekema, and Johnothan Van Why) and Carnegie Mellon (Hartmut Geyer, William Martin, and Albert Wu) DRC team members. The authors are especially thankful to Andrew Peekema and Mikhail Jones for implementing the controller and running the experiments, William Martin for building the simulation environment, and Christian Hubicki for editing the Youtube videos and maintaining the channel.

Funding

This research was funded by the DARPA Maximum Mobility and Manipulation Program, grants W31P4Q-13-C-0099 and W91CRB-11-1-0002.

References

Altendorfer R, Koditschek D and Holmes P (2004) Stability analysis of legged locomotion models by symmetry-factored return maps. *The International Journal of Robotics Research* 23(10-11): 979–999.

Bernstein DS (2009) *Matrix mathematics: theory, facts, and formulas*. Princeton, NJ: Princeton university press.

Blickhan R (1989) The spring-mass model for running and hopping. *Journal of Biomechanics* 22(11-12): 1217–1227.

Blickhan R and Full RJ (1993) Similarity in multilegged locomotion: bouncing like a monopode. *Journal of Comparative Physiology A* 173(5): 509–517.

Borgmann A, Hooper SL and Büschges A (2009) Sensory feedback induced by front-leg stepping entrains the activity of central pattern generators in caudal segments of the stick insect walking system. *Journal of Neuroscience* 29(9): 2972–2983.

Cham JG and Cutkosky MR (2007) Dynamic stability of open-loop hopping. *Journal of dynamic systems, measurement, and control* 129(3): 275–284.

Da X and Grizzle J (2019) Combining trajectory optimization, supervised machine learning, and model structure for mitigating the curse of dimensionality in the control of bipedal robots. *The International Journal of Robotics Research* 38(9): 1063–1097.

Daley MA and Biewener AA (2006) Running over rough terrain reveals limb control for intrinsic stability. *Proceedings of the National Academy of Sciences* 103(42): 15681–15686.

De A and Koditschek D (2015) The penn jerboa: A platform for exploring parallel composition of templates. *arXiv preprint arXiv:1502.05347* .

DRL (2015a) ATRIAS bipedal robot: Takes a walk in the park. URL https://www.youtube.com/watch?v=dl7KUUVHC-M. Dynamic Robotics Laboratory.

DRL (2015b) ATRIAS robot: 9.1 kph running speed (5.7 mph). URL https://www.youtube.com/watch?v=U4eBRPHYCdA. Dynamic Robotics Laboratory.

DRL (2015c) ATRIAS robot: Climbs a 15-cm obstacle. URL https://www.youtube.com/watch?v=dOoQTPqnLqI. Dynamic Robotics Laboratory.

DRL (2015d) ATRIAS robot: Dodgeball barrage. URL https://www.youtube.com/watch?v=yYvrTc3-uVU. Dynamic Robotics Laboratory.

DRL (2015e) ATRIAS robot: Gets kicked. URL https://www.youtube.com/watch?v=5BF3uzXWfDY. Dynamic Robotics Laboratory.

DRL (2015f) ATRIAS robot: Runs to the end zone. URL https://www.youtube.com/watch?v=KeSkAPYAJc4. Dynamic Robotics Laboratory.

DRL (2015g) ATRIAS robot: Sidestepping. URL https://www.youtube.com/watch?v=yd4zTfjd0LI. Dynamic Robotics Laboratory.

DRL (2015h) ATRIAS robot: Traverses rough terrain at 6.6 kph (4.1 mph). URL https://www.youtube.com/watch?v=VBDysRlrfcY. Dynamic Robotics Laboratory.

DRL (2015i) Stand to walk (testing) 2015-01-15. URL https://www.youtube.com/watch?v=XwgFMjmVoUM. Dynamic Robotics Laboratory.

Elery T, Rezazadeh S, Nesler C, Doan J, Zhu H and Gregg RD (2018) Design and benchtop validation of a powered knee-ankle prosthesis with high-torque, low-impedance actuators. In: *IEEE International Conference on Robotics and Automation (ICRA)*. Brisbane, Australia.

Ernst M, Geyer H and Blickhan R (2009) Spring-legged locomotion on uneven ground: a control approach to keep the running speed constant. In: *International Conference on Climbing and Walking Robots (CLAWAR)*. Istanbul, Turkey, pp. 639–644.

Farley CT and Ferris DP (1998) Biomechanics of walking and running: from center of mass movements to muscle action. *Exercise and sport sciences reviews* 26(1): 253–286.

Fleishman B (1965) Forced oscillations and convex superposition in piecewise-linear systems. *Siam Review* 7(2): 205–222.

Full RJ and Koditschek D (1999) Templates and anchors: neuromechanical hypotheses of legged locomotion on land. *Journal of Experimental Biology* 202(23): 3325–3332.

Garofalo G, Ott C and Albu-Schäffer A (2012) Walking control of fully actuated robots based on the bipedal slip model. In: *IEEE International Conference on Robotics and Automation (ICRA)*. Saint Paul, MN, pp. 1456–1463.

Geyer H, Blickhan R and Seyfarth A (2002) Natural dynamics of spring-like running: Emergence of selfstability. In: *5th International Conference on Climbing and Walking Robots*. Suffolk, UK, pp. 87–91.

Geyer H, Seyfarth A and Blickhan R (2005) Spring-mass running: simple approximate solution and application to gait stability. *Journal of theoretical biology* 232(3): 315–328.

Geyer H, Seyfarth A and Blickhan R (2006) Compliant leg behaviour explains basic dynamics of walking and running. *Proceedings of the Royal Society B: Biological Sciences* 273(1603): 2861–2867.

Griffin B and Grizzle J (2017) Nonholonomic virtual constraints and gait optimization for robust walking control. *The International Journal of Robotics Research* 36(8): 895–922.

Haldane DW, Plecnik M, Yim JK and Fearing RS (2016) Robotic vertical jumping agility via series-elastic power modulation. *Science Robotics* 1(1).

Hereid A, Kolathaya S, Jones MS, Van Why J, Hurst JW and Ames AD (2014) Dynamic Multi-domain Bipedal Walking with ATRIAS Through SLIP Based Human-inspired Control. In: *Proceedings of the 17th International Conference on Hybrid Systems: Computation and Control*. Berlin, Germany, pp. 263–272.

Hogan N (1985) Impedance Control: An Approach to Manipulation: Part I—Theory. *Journal of Dynamic Systems, Measurement, and Control* 107(1): 1–7.

Hubicki C, Abate A, Clary P, Rezazadeh S, Jones M, Peekema A, Van Why J, Domres R, Wu A, Martin W et al. (2018) Walking and Running with Passive Compliance: Lessons from Engineering: A Live Demonstration of the ATRIAS Biped. *IEEE Robotics & Automation Magazine* 25(3): 23–39.

Hubicki C, Grimes J, Jones M, Renjewski D, Spröwitz A, Abate A and Hurst J (2016) ATRIAS: Design and validation of a tether-free 3d-capable spring-mass bipedal robot. *The International Journal of Robotics Research* 35(12): 1497–1521.

Jindrich DL and Full RJ (2002) Dynamic stabilization of rapid hexapedal locomotion. *Journal of Experimental Biology* 205(18): 2803–2823.

Kemper K, Koepl D and Hurst JW (2010) Optimal passive dynamics for torque/force control. In: *IEEE International Conference on Robotics and Automation (ICRA)*. Anchorage, AK, pp. 2149–2154.

Khalil HK (1996) *Noninear systems*. Princeton, NJ: Prentice-Hall.

Kim D, Zhao Y, Thomas G, Fernandez BR and Sentis L (2016) Stabilizing series-elastic point-foot bipeds using whole-body operational space control. *IEEE Transactions on Robotics* 32(6): 1362–1379.

Koditschek D and Buehler M (1991) Analysis of a simplified hopping robot. *The International Journal of Robotics Research* 10(6): 587–605.

Komsuoglu H and Koditschek D (2000) Preliminary analysis of a biologically inspired 1-dof 'clock' stabilized hopper. In: *Proceedings of World Multiconference on Systemics, Cybernetics and Informatics*. Orlando, FL, pp. 670–675.

Koolen T, De Boer T, Rebula J, Goswami A and Pratt J (2012) Capturability-based analysis and control of legged locomotion, part 1: Theory and application to three simple gait models. *The International Journal of Robotics Research* 31(9): 1094–1113.

Lipfert SW, Günther M, Renjewski D and Seyfarth A (2014) Impulsive ankle push-off powers leg swing in human walking. *Journal of experimental biology* 217(8): 1218–1228.

Lohmiller W and Slotine JJE (1998) On contraction analysis for non-linear systems. *Automatica* 34(6): 683–696.

Martin WC, Wu A and Geyer H (2015) Robust spring mass model running for a physical bipedal robot. In: *IEEE International Conference on Robotics and Automation (ICRA)*. Seattle, WA, pp. 6307–6312.

Martinez H and Carbajal J (2011) From walking to running a natural transition in the SLIP model using the hopping gait. In: *IEEE International Conference on Robotics and Biomimetics (ROBIO)*. Phuket, Thailand, pp. 2163–2168.

Natsiavas S (1989) Periodic response and stability of oscillators with symmetric trilinear restoring force. *Journal of Sound and Vibration* 134(2): 315–331.

Park HW, Ramezani A and Grizzle J (2013) A finite-state machine for accommodating unexpected large ground-height variations in bipedal robot walking. *IEEE Transactions on Robotics* 29(2): 331–345.

Pogorilyi O, Jazar RN, and Trivailo PM (2015) Challenges in exact response of piecewise linear vibration isolator. In: Dai L and Jazar RN (eds.) *Nonlinear Approaches in Engineering Applications*, chapter 3. Heidelberg, Germany: Springer.

Post DC and Schmiedeler JP (2014) Velocity disturbance rejection for planar bipeds walking with hzd-based control. In: *IEEE/RSJ International Conference on Intelligent Robots and Systems (IROS)*. Chicago, IL, pp. 4882–4887.

Poulakakis I and Grizzle J (2009) The spring loaded inverted pendulum as the hybrid zero dynamics of an asymmetric hopper. *IEEE Transactions on Automatic Control* 54(8): 1779–1793.

Pratt J, Carff J, Drakunov S and Goswami A (2006) Capture point: A step toward humanoid push recovery. In: *6th IEEE-RAS International Conference on Humanoid Robots*. Genova, Italy, pp. 200–207.

Proctor J and Holmes P (2010) Reflexes and preflexes: on the role of sensory feedback on rhythmic patterns in insect locomotion. *Biological cybernetics* 102(6): 513–531.

Raibert M (1986) *Legged robots that balance*. Cambridge, MA: MIT Press.

Reher J, Cousineau EA, Hereid A, Hubicki CM and Ames AD (2016) Realizing dynamic and efficient bipedal locomotion on the humanoid robot durus. In: *IEEE International Conference on Robotics and Automation (ICRA)*. Stockholm, Sweden, pp. 1794–1801.

Rezazadeh S, Abate A, Hatton RL and Hurst JW (2018) Robot leg design: A constructive framework. *IEEE Access* 6(1): 54369–54387.

Rezazadeh S and Gregg RD (2016) A control framework for anthropomorphic biped walking based on stabilizing feedforward trajectories. In: *ASME Dynamic Systems and Control Conference (DSCC)*. Minneapolis, MN, p. V001T06A007.

Rezazadeh S, Hubicki C, Jones M, Peekema A, Van Why J, Abate A and Hurst J (2015) Spring-Mass Walking With ATRIAS in 3D: Robust Gait Control Spanning Zero to 4.3 KPH on a Heavily Underactuated Bipedal Robot. In: *ASME Dynamic Systems and Control Conference (DSCC)*. Columbus, OH, p. V001T04A003.

Rezazadeh S and Hurst JW (2015) Toward step-by-step synthesis of stable gaits for underactuated compliant legged robots. In: *IEEE International Conference on Robotics and Automation (ICRA)*. Seattle, WA, pp. 4532–4538.

Schaal S and Atkeson CG (1993) Open loop stable control strategies for robot juggling. In: *Proceedings IEEE International Conference on Robotics and Automation (ICRA)*, volume 3. Atlanta, GA, pp. 913–918.

Schmitt J (2006) A simple stabilizing control for sagittal plane locomotion. *Journal of computational and nonlinear dynamics* 1(4): 348–357.

Schmitt J and Clark J (2009) Modeling posture-dependent leg actuation in sagittal plane locomotion. *Bioinspiration & Biomimetics* 4(4): 046005.

Schulman J (1983) Chaos in piecewise-linear systems. *Physical review A* 28(1): 477–480.

Schwind WJ and Koditschek D (1995) Control of forward velocity for a simplified planar hopping robot. In: *Proceedings of IEEE International Conference on Robotics and Automation (ICRA)*, volume 1. Nagoya, Japan, pp. 691–696.

Seyfarth A (2003) Swing-leg retraction: a simple control model for stable running. *Journal of Experimental Biology* 206(15): 2547–2555.

Seyfarth A, Geyer H, Günther M and Blickhan R (2002) A movement criterion for running. *Journal of Biomechanics* 35(5): 649–655.

Spong MW (1994) Partial feedback linearization of underactuated mechanical systems. In: *Proceedings of the IEEE/RSJ/GI International Conference on Intelligent Robots and Systems (IROS) 'Advanced Robotic Systems and the Real World'*, volume 1. Munich, Germany, pp. 314–321.

Sreenath K, Park HW, Poulakakis I and Grizzle JW (2011) A compliant hybrid zero dynamics controller for stable, efficient and fast bipedal walking on mabel. *The International Journal of Robotics Research* 30(9): 1170–1193.

Vejdani HR, Wu A, Geyer H and Hurst JW (2015) Touch-down angle control for spring-mass walking. In: *IEEE International Conference on Robotics and Automation (ICRA)*. Seattle, WA, pp. 5101–5106.

Vose TH, Umbanhowar P and Lynch KM (2012) Sliding manipulation of rigid bodies on a controlled 6-dof plate. *The International Journal of Robotics Research* 31(7): 819–838.

Wensing PM and Orin DE (2013) High-speed humanoid running through control with a 3d-slip model. In: *IEEE/RSJ International Conference on Intelligent Robots and Systems (IROS)*. Tokyo, Japan, pp. 5134–5140.

Westervelt ER, Chevallereau C, Choi JH, Morris B and Grizzle JW (2007) *Feedback control of dynamic bipedal robot locomotion*. Boca Raton, FL: CRC press.

Whittaker ET (1917) *A treatise on the analytical dynamics of particles and rigid bodies*. Second edition. Cambridge, UK: Cambridge University Press.

Wu A and Geyer H (2013) The 3-d spring–mass model reveals a time-based deadbeat control for highly robust running and steering in uncertain environments. *IEEE Transactions on Robotics* 5(29): 1114–1124.

Zelik KE, Huang TWP, Adamczyk PG and Kuo AD (2014) The role of series ankle elasticity in bipedal walking. *Journal of theoretical biology* 346: 75–85.